

Penetration and aerosolization of cough droplet spray through face masks: A unique pathway of transmission of infection


Cite as: Phys. Fluids **34**, 052108 (2022); <https://doi.org/10.1063/5.0093297>


Submitted: 28 March 2022 • Accepted: 22 April 2022 • Published Online: 10 May 2022

 Gautham Vadlamudi, S. K. Thirumalaikumaran,  Dipshikha Chakravorty, et al.

COLLECTIONS

Paper published as part of the special topic on [Flow and the Virus](#)

 This paper was selected as Featured

 This paper was selected as Scilight



View Online



Export Citation



CrossMark

ARTICLES YOU MAY BE INTERESTED IN

[Perimeter leakage of face masks and its effect on the mask's efficacy](#)

Physics of Fluids **34**, 051902 (2022); <https://doi.org/10.1063/5.0086320>

[Efficacy of homemade face masks against human coughs: Insights on penetration, atomization, and aerosolization of cough droplets](#)

Physics of Fluids **33**, 093309 (2021); <https://doi.org/10.1063/5.0061007>

[On respiratory droplets and face masks](#)

Physics of Fluids **32**, 063303 (2020); <https://doi.org/10.1063/5.0015044>



Physics of Fluids

Special Topic: Paint and Coating Physics

Submit Today!

Penetration and aerosolization of cough droplet spray through face masks: A unique pathway of transmission of infection



Cite as: Phys. Fluids **34**, 052108 (2022); doi: [10.1063/5.0093297](https://doi.org/10.1063/5.0093297)

Submitted: 28 March 2022 · Accepted: 22 April 2022 ·

Published Online: 10 May 2022



View Online



Export Citation



CrossMark

Gautham Vadlamudi,¹ S. K. Thirumalaikumaran,¹ Dipshikha Chakravorty,^{2,3} Abhishek Saha,⁴ and Saptarshi Basu^{1,5,a)}

AFFILIATIONS

¹Department of Mechanical Engineering, Indian Institute of Science, Bangalore, Karnataka 560012, India

²Department of Microbiology and Cell Biology, Indian Institute of Science, Bangalore, Karnataka 560012, India

³Center of Biosystems Science and Engineering, Indian Institute of Science, Bangalore, Karnataka 560012, India

⁴Department of Mechanical and Aerospace Engineering, University of California San Diego, La Jolla, California 92093, USA

⁵Interdisciplinary Centre for Energy Research (ICER), Indian Institute of Science, Bangalore, Karnataka 560012, India

Note: This paper is part of the special topic, Flow and the Virus.

^{a)}Author to whom correspondence should be addressed: sbasu@iisc.ac.in

ABSTRACT

The advent of the COVID-19 pandemic has necessitated the use of face masks, making them an integral part of the daily routine. Face masks occlude the infectious droplets during any respiratory event contributing to source control. In the current study, spray impingement experiments were conducted on porous surfaces like masks having a different porosity, pore size, and thickness. The spray mimics actual cough or a mild sneeze with respect to the droplet size distribution (20–500 μm) and velocity scale (0–14 m/s), which makes the experimental findings physiologically realistic. The penetration dynamics through the mask showed that droplets of all sizes beyond a critical velocity penetrate through the mask fabric and atomize into daughter droplets in the aerosolization range, leading to harmful effects due to the extended airborne lifetime of aerosols. By incorporating spray characteristics along with surface tension and viscous dissipation of the fluid passing through the mask, multi-step penetration criteria have been formulated. The daughter droplet size and velocity distribution after atomizing through multi-layered masks and its effects have been discussed. Moreover, the virus-emulating particle-laden surrogate respiratory droplets are used in impingement experiments to study the filtration and entrapment of virus-like nanoparticles in the mask. Furthermore, the efficacy of the mask from the perspective of a susceptible person has been investigated.

Published under an exclusive license by AIP Publishing. <https://doi.org/10.1063/5.0093297>

NOMENCLATURE

A_{mask}	Area of mask
A_p	Individual pore area
A_{pores}	Net pore area
$A_{\text{spray } c/s}$	Net cross-sectional projected area of spray droplets
d	Droplet diameter
E_d	Viscous dissipation
E_k	Kinetic energy
h	Dimension of fabric sample under consideration
Re	Reynolds number
t_m	Fabric thickness
V	Impact velocity
We	Weber number

Symbols

σ	Surface tension
ϕ	Porosity
ϵ	Pore size
ρ	Liquid density
μ	Dynamics viscosity
\mathbb{C}	Cross-sectional spray areal density

I. INTRODUCTION

The transportation of pathogen-loaded respiratory droplets from an infected person to a susceptible person can potentially trigger a global pandemic such as COVID-19.^{1–3} The respiratory droplets are ejected from an infected person during breathing, talking, singing,

spitting, coughing, or sneezing, which can contribute to the spread of the virus into the surroundings. These droplets can lead to infection when inhaled through the oral or nasal passages of a healthy person.⁴ In the case of larger size droplets ($>100\ \mu\text{m}$), the ejected droplets can settle on the surfaces as fomites^{5,6} following the ballistic trajectory, exhibiting a shorter airborne lifetime as represented using Wells curve.⁷ The intermediate-sized droplets may get transported over significant distances, and the smaller droplets ($5\text{--}10\ \mu\text{m}$) remain suspended in the air for even longer durations. These smaller droplets may evaporate, crystallize into nuclei, and transport from place to place by air flow.^{8,9} The spread and infection probability due to the ejected droplets depend on the droplet size and ambient conditions. Chaudhuri *et al.* estimated that the droplets in the range of $10\text{--}50\ \mu\text{m}$ have high infection potential. Blocking the droplets above the range of $10\ \mu\text{m}$ with both face mask usage and social distancing may help in restricting the spread of highly infectious diseases, such as COVID-19.^{10,11}

The face masks primarily contribute as a source control mechanism and act as a physical barrier to the release of virus-loaded respiratory droplets into the surroundings.¹² MacIntyre *et al.* conducted clinical trials of face mask usage, tracking the spread of different respiratory viruses. It was concluded that there is a relative reduction of about 60%–80% in transmission with adherent mask usage.¹³ Another critical aspect of the study is that even with different transmission mechanisms like large droplets, aerosol, or fomite, all major viruses are transmitted through the respiratory route, which can be reduced with mask usage. However, the relative effectiveness depends on the mask's type and properties, which further reduces the distance traveled by the droplets.¹⁴ Konda *et al.* investigated the filtration efficiencies of several standard fabrics, including cotton, silk, chiffon, flannel, various synthetics, and their combinations in multi-layered configurations using polydisperse NaCl aerosols.¹⁵

Droplet fragmentation studies through a mesh have been performed by researchers to study the penetration modes, ejection angle, single-hole mass transfer, and mesh properties.^{16–18} Brunet *et al.* proposed method to produce monodisperse spray having individual droplets up to pico-liters of volume.¹⁶ Lewei *et al.* showed that the mass transfer ratio and ejection angle can be approximated as a function of a modified Weber number.¹⁷ The microdroplet impact on superhydrophobic surfaces and meshes has been studied.^{19–21} Sun *et al.* showed different types of penetrated spray formation during different stages of droplet impingement on superhydrophobic surfaces.¹⁹ Ryu *et al.* showed that a different wettability, that is, superhydrophobicity and hydrophobicity, leads to different penetration dynamics of impinging droplet through a mesh.²² Researchers have conducted droplet impact studies using porous networks like metallic wire meshes, fibers, and textiles. They showed that the penetration characteristics depend on surface wettability, impact velocity, mesh size, and fluid properties.^{23–26} However, Sahu *et al.* showed that beyond a critical impact velocity, penetration would occur through fiber pores irrespective of wettability²⁷ and drop size. Xu *et al.* studied the effect of number of pores (N), water hammer pressure, and advancing contact angle in the case of single-droplet impingement on mesh.²⁸ Kooij *et al.* studied the ligament breakup and droplet fragmentation after impacting on a mesh. They showed that the breakup is controlled by the instabilities arising due to initial perturbations in the droplet.²³ Krishan *et al.* have conducted experiments of droplet impingement on cotton and surgical masks, concluding that fabric properties like pore size and porosity affect the droplet penetration criteria.²⁹ Sharma *et al.*

focused on the effect of the number of layers present in a surgical mask. They showed that the volume of daughter droplets was significantly reduced after penetration in the presence of an additional layer.³⁰ Bagchi *et al.* have investigated the droplet impingement on wet facemasks to study the penetration and secondary atomization phenomena.³¹

Arumuru *et al.* have determined the average distance traveled by the sneeze droplets with different combinations of face masks and face shields using jet visualization.³² Verma *et al.* have investigated the efficacy of different commercially available face masks by determining the distance traveled by the respiratory jets.³³ Many investigations have been conducted by researchers to test the efficacy of masks, all of which primarily focused on smaller-sized droplets ($0\text{--}100\ \mu\text{m}$).^{14,34–37} Flow-field generated by coughing with and without surgical masks has been investigated by Kahler and Hain to study the flow blockage caused by the masks using PIV measurements.³⁷ Optical Schlieren experiments conducted by Tang *et al.* showed that the forward jet of droplets during a coughing event is blocked by the mask; however, leakage around the top, bottom, and sides is observed.³⁶ Manikin experiments are done by Pan *et al.* to evaluate the inward and outward effectiveness of cloth masks, surgical masks, and face shields using aerosol generators. The filtration efficiency has been measured using an aerodynamic particle sizer spectrometer connected to the inhaling manikin. They recommended the usage of a three-layered mask consisting of outer layers of a flexible, tightly woven fabric and an inner layer consisting of a material designed to filter out particles.³⁸ Rothamer *et al.* have also performed manikin studies to evaluate the impact of ventilation on aerosol dynamics in a classroom setting. They have studied the filtration efficiency of different types of masks. It showed that high filtration efficient masks are necessary to reduce the infection probability, as the effect of ventilation alone is not enough to control the spread.³⁹ The effectiveness of blocking virus-like nanoparticles by standard fabrics has been investigated by Lustig *et al.*⁴⁰ The mask efficiency, leakage, and filtration for multiple cough cycles during mild cough have been investigated by Dbouk and Drikakis.⁴¹ The mechanism of interception of respiratory droplets in fibrous porous media of face mask has been investigated by Maggiolo and Sasic. It is shown that the efficiency of fibrous media intercepting droplets for a given droplet-to-fiber size ratio can be estimated using a parameter that is a function of porosity.⁴²

It is reported that the saliva droplets ejected from a human cough can travel up to a distance of 2 m with zero wind speed, and the range may increase to 6 m with a wind speed of 4–15 km/h.⁴³ Studies have been conducted by Lindsley *et al.* using cough simulators, which can generate an airflow of 32 m/s having cough aerosol particles ($0\text{--}100\ \mu\text{m}$).⁴⁴ It is to be noted that the respiratory droplets during a cough are characterized by a wide range of sizes, from submicrometer to few millimeters^{9,36,45} with an average velocity of 10 m/s.^{46,47} Even though the number of large-sized droplets ($>250\ \mu\text{m}$) is small in a cough, a significantly large percentage of total expelled volume (94.21%) is contributed by these larger droplets.⁹ Duguid has shown a direct correlation between the amount of pathogen loading and the droplet volume. This suggests that these larger-sized droplets are also relevant in disease transmission along with the aerosolized droplets ($<100\ \mu\text{m}$). Furthermore, Yan *et al.* showed that large droplets are also produced during both sneezing and coughing, along with the aerosol.⁴⁸ It is shown that the aerosol and particle filtration efficiency

of a mask depends on the fabric material porosity, thickness, fiber diameter, and single-fiber efficiency of filtration. The single-fiber filtration efficiency is the collective sum of the efficiencies of diffusion, interception, impaction, and electrostatic deposition of the particles on the fiber, all of which are not purely hydrodynamic in nature.⁴⁹

Most of the aforementioned experimental investigations on masks involved the study of flow-field and aerosolized jets at similar Reynolds numbers associated with the actual cough or sneeze. These studies focused on the distance traveled by the droplets or its correlation with different types of masks: the effect of mask fit or ventilation. The individual droplet impact studies in the literature were primarily focused on the larger droplets and their penetration criteria on different meshes or fabrics. However, as discussed before, both larger and smaller droplets are produced during a coughing or a sneezing event. The droplet size is essential as the size of the droplet determines the mode of infection transmission (settling or aerosol transport or fomites).^{29,30} Even though the larger-sized droplets potentially containing more viral loadings are blocked by the mask,³⁵ they can atomize into the aerosolization range leading to infection spread. This necessitates the investigation of the atomization mechanism of impinging droplets, daughter droplet size distribution, and the effect of mask properties. Furthermore, most of the manikin studies in the literature mainly focused on the filtration aspect of the mask but not the atomization phenomenon involved during the penetration of the droplets. The spray impingement with a droplet size range of 0–500 μm impinging on a mask surface with a velocity of 10 m/s closely resembles the characteristics of an actual cough or a mild sneeze that is rarely studied in the literature.

A fundamental study on the spray impingement offers insight into the droplet penetration criteria, the possibility of secondary atomization, ligament formation, ligament breakup, and size distribution of the daughter droplets. These hydrodynamic aspects of droplet–mask interaction are investigated without the burst of air involved during a cough. Additionally, it provides insight into how the mask properties like porosity, pore size, and the number of layers affect these phenomena. In our previous studies, the single-droplet impingement has been studied to get insight into the penetration phenomenon locally.^{29,30} In continuation, an experimental investigation has been conducted in the current study replicating a model-cough by impinging a spray with similar droplet size and velocity range associated with actual cough. The effect of different fabric properties of mask samples on penetration dynamics has been addressed. Based on the spray impingement experiments, the penetration dynamics of different-sized droplets present in the spray of a cough are also investigated. Further, the filtration of virus-emulating nanoparticles and the deposition of nanoparticles on mask surface have been studied. Experiments have been conducted to study the fate of penetrated respiratory cough droplets from an infected person wearing a mask in the presence of a susceptible person in proximity. This provides insight into the effect of mask usage on both ends, that is, the infected person and the susceptible person.

II. MATERIALS AND METHODS

A. Experimental setup

The experimental investigation has been conducted to study the efficacy and penetration criteria for a model-cough (spray) impingement on mask surface using high-speed shadowgraphy imaging. The cough or sneeze event is simulated with DI water spray. The spray is

generated using a pressurized liquid chamber, a nozzle orifice, and a solenoid valve. Arduino code is used to actuate the solenoid valve for a specific opening time. When triggered, the solenoid valve opens and closes based on the preset time delay, allowing the pressurized DI water to be ejected from the nozzle in the form of a spray. It must be noted that the respiratory droplet velocity and size vary depending on the specific event: normal breathing, coughing, sneezing, etc. In this study, the velocity scale and droplet sizing of the incident spray are maintained in the range corresponding to respiratory droplets involved in actual cough or mild sneezing events, as indicated in the literature.⁹ In current experiments, the droplet velocity range is around 10 m/s with maximum velocity reaching up to 14 m/s and the droplet diameter distribution range of 0–600 μm , peaking around 60–70 μm , similar range as shown by Duguid⁹ (see the [supplementary material Fig. S1](#)). Additionally, the spray cone size at the point of impact on the mask is set to be in the range of ~ 3 –4 cm, as shown for typical cough droplets.^{41,43} It is to be noted that the current study primarily focuses on the hydrodynamic aspects of the phenomenon, by investigating the effects of high-speed droplets during cough events.

The global characteristics of spray impingement through a mask have been investigated using a manikin head with the aforementioned nozzle orifice used as the source of the spray from the mouth opening (see [Fig. 1](#)). The effort has been made to replicate the spray similar to that of an actual cough or sneeze as explained before, by matching the parameters like droplet size, velocity range, and spray size. The main objective is to check for the penetration characteristics and get comprehensive insight into the spray impingement and penetration phenomena. An actual spray is used for impingement in the current study instead of a single droplet, which has been investigated in our previous work. Using a manikin, the spray penetration characteristics have been investigated qualitatively. The physical proximity and dimensions with the manikin and spray are maintained similar to that of an actual human cough, with and without wearing a mask.

Additionally, a local investigation has been conducted to check the spray impingement phenomenon quantitatively on the mask layers that are mounted on a post. A more fundamental approach has been taken to study the correlation between mask morphological characteristics and penetration characteristics like the size and velocity distribution of the penetrated daughter droplets. The effect of the presence of multiple layers on the spray impingement has also been investigated in detail with different combinations of mask samples. DI water has been used to mimic the respiratory droplet spray ejected onto the inner side of the mask from an infected person (see [Fig. 1](#)). The surface tension of DI water ($\sigma = 72 \text{ Mn/m}$) was found to be similar to that of cough droplets ($\sigma = 65.9 \text{ Mn/m}$).^{30,50} However, the other fluid properties may vary between the model-cough droplets used and the actual cough droplets. Nevertheless, in the scope of current study of spray droplet penetration, only surface tension, viscosity, and viscoelasticity are relevant fluid properties. Furthermore, it has been shown that the effect of the droplet fluid properties on penetration becomes less critical at high-impact velocities ($\sim 10 \text{ m/s}$).⁵¹ Additional experiments with surrogate respiratory liquid (0.9% by wt. % NaCl, 0.3% by wt. % gastric mucin, 0.05% by wt. % DPPC added to DI water, i.e., mucin solution) have been conducted.^{30,52} It showed no noticeable difference in the penetration characteristics, suggesting an insignificant influence of droplet fluid properties at high-impact velocities. Hence, DI water has been used for spray impingement experiments.

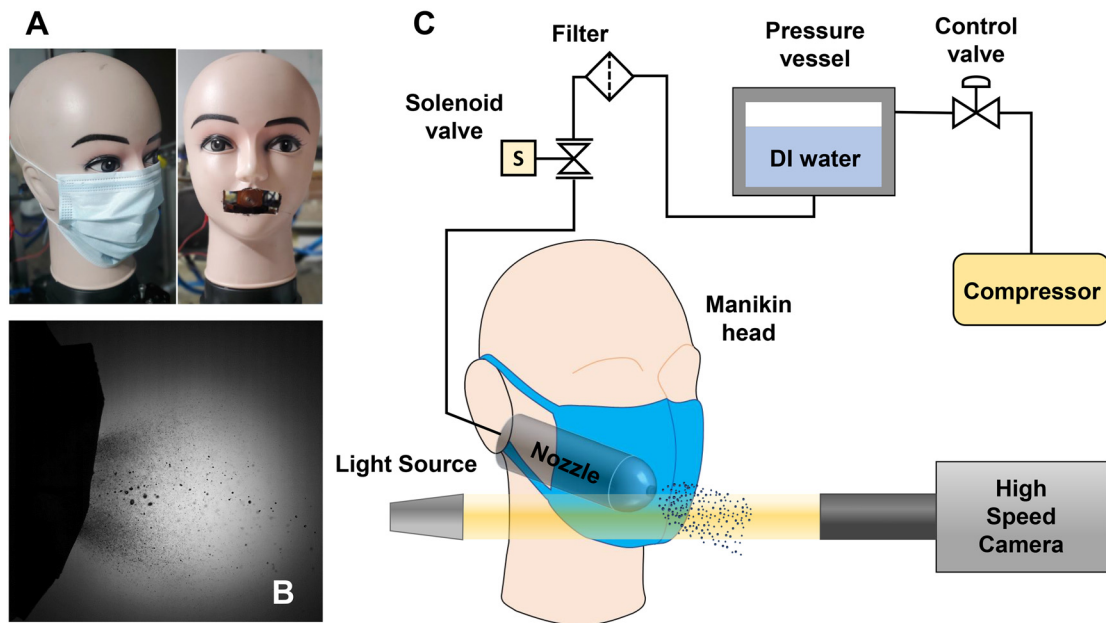


FIG. 1. (a) Manikin with and without mask. Spray nozzle orifice is shown on the right side. (b) Shadowgraphy image showing the daughter droplets after penetration for layer A. (c) Manikin experimental setup: high-speed cameras were used to capture the side view of the manikin experiments for different mask samples. Pressurized DI water is connected to the nozzle through a solenoid valve.

In addition to that, experiments have been performed using the virus-emulated nanoparticle-laden surrogate respiratory liquid (mucin solution), to generate a model-cough spray for impingement.^{5,30} The properties of mucin solution used are in similar to that of DI water. The dynamic viscosity of mucin solution is measured to be $\mu \sim 0.98$ mPa s, using a rheometer. The 100 nm sized R-100 polystyrene nanoparticles were used as a model material for the viral loading based on similarity in geometrical properties (although they differ in biological and chemical properties).⁶ Further, the filtration of viral loading by the mask has been investigated using the nanoparticle-laden surrogate respiratory liquid at a different particle loading. Experiments have been further conducted, by placing a second manikin (representing a susceptible person with and without the mask) in the path of penetrated droplets ejected from the primary manikin (infected person), to check the effect of mask usage by the susceptible person.

B. High-speed shadowgraphy

A high-speed camera (Photron SA5) coupled with TOKINA MACRO 100 F2.8 with a 36 mm extension tube (for side view) has been used to focus on the plane of descent of the spray (see Fig. 2). The side view of the spray impingement has been captured using a mercury lamp light source as backlighting to study the penetration dynamics. The camera acquisition rate was kept at 10 000 frames per second with a shutter speed of 93 000 cycles per second for the shadowgraphy imaging, at a resolution of 896×848 , as shown in Fig. 2. Due to experimental limitations, uncertainty in the measurement of droplet size is minimized by using adaptive thresholding to avoid the

highly out-of-focus stray droplets. The droplets' size and velocity were determined using object detection on the shadowgraphy images by binarizing the raw images with adaptive thresholding. From this, the line-of-sight area of the droplets can be obtained from which the equivalent diameter is calculated to estimate the volume of each droplet. The data processing has been performed for 20 experimental runs for each case in order to obtain the probability distribution function of the droplet size as well as the droplet velocity. The uncertainty in droplet diameter measurement is $\pm 23.8 \mu\text{m}$, and velocity measurement is ± 0.12 m/s. It is to be noted that only those set of frames were considered for data measurements in which the spray inlet distribution is similar to that in the literature for actual cough droplets.⁹

C. Mask sample characterization

In the current study, different layers (referred to as layers A, B, C) used in commercially available standard surgical masks have been considered as test samples that have a varied range of properties like porosity (ϕ), fabric thickness (t_m), and pore size (ϵ). Experimental investigation has been conducted using different combinations of these samples in single-, double-, and triple-layer configurations. The samples were characterized based on the aforementioned properties like pore size and porosity, which were calculated from the magnified cross-sectional shadowgraphy images of the samples, as shown in Fig. 3. Thresholding and binarization have been performed on these images to get the net area of the empty gaps or spaces available in the fabric sample (A_{pores}).

The ratio of the net pore area obtained (A_{pores}) and the total area of the fabric sample under consideration (h^2) gives the value of porosity (ϕ) for the corresponding sample. The pore size (ϵ) is obtained

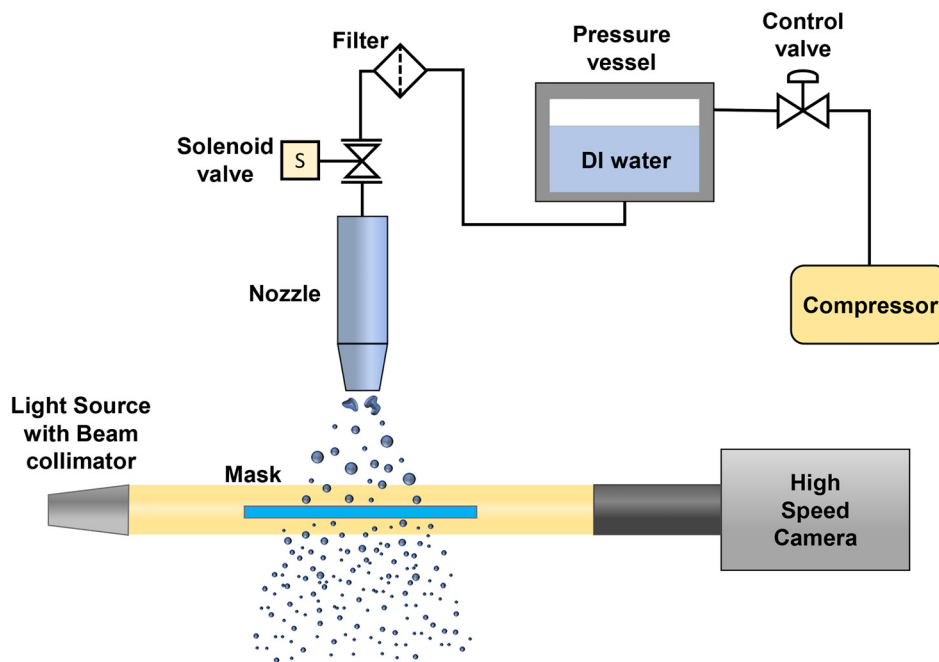


FIG. 2. The experimental setup used for the fundamental investigation: high-speed cameras were used to capture the side view of the spray impinging on the surface of different mask samples. A high-intensity light source has been used to capture the high-speed dynamics of spray impact.

from the individual pore area A_p , which is the ratio of A_{pores} and total number of pores present. With the addition of an extra layer, the amount of gap or pores available in the sample for the droplets to pass will decrease. Hence, the effective value of porosity and pore size is considered using a similar method for multi-layered samples as well. The different test cases considered in this study with the sample properties in single-, double-, and triple-layer configurations are given in Table I. It is to be noted that the multilayer configuration of layer B has not been considered because layer B alone has a very low value of porosity, which leads to negligible effective porosity when used in multilayer configuration.

III. RESULTS AND DISCUSSION

Model-cough is produced using a spray nozzle orifice by maintaining the droplet velocity reaching the maximum value of 14 m/s, and droplet sizes ranging from 0 to 600 μm peaking around 60–70 μm , similar to the characteristics of respiratory droplets ejected during a cough or mild sneeze, as shown by Duguid⁹ (see Fig. S1) and other researchers in the literature.^{36,45} The spray nozzle is mounted in the mouth of a manikin to study the mask efficacy in blocking the cough droplets and to study the mechanism of droplet penetration and atomization. Figure 4(a) shows the schematic of shadowgraphy image of spray droplets ejected from the nozzle before and after penetration. Different mask samples (see Sec. II) were used to study the effect of mask properties like porosity (ϕ), pore size (ϵ), and thickness (t_m) on the droplet penetration dynamics. Experiments conducted showed that the spray impingement, penetration dynamics, and penetrated droplet size distribution are similar, while using either DI water or surrogate respiratory droplet with virus-emulating nanoparticles (mucin solution + nanoparticles) as the impinging fluid, as shown in Figs. 4(b) and 4(c) (see Sec. II). The different sizes of droplets present in the spray atomize into smaller daughter droplets as they pass

through the fabric pores, through ligament formation and secondary atomization, as shown in Fig. 4(d).

Since it has been shown that the penetration dynamics are similar for DI water and respiratory droplets, especially at high impingement velocities,^{30,50} the experiments were conducted with DI water using different mask samples as shown in Sec. II. Figures 5(a)–5(g) (multimedia view) show the shadowgraphy images of the model-cough impingement generated using a nozzle orifice fitted inside the mouth of a manikin wearing different mask samples. Figure 5(a) shows the model-cough spray coming out of the manikin's mouth opening, and it is evident from the image that the spray consists of droplets having a wide range of sizes. The cone angle of the spray is shown in the figure as well [see Fig. 5(a)]. Since manikin head has been used, the spray coming out of the mouth exhibits a more realistic behavior by interacting with the manikin's mouth edges leading to other effects like secondary breakup-like phenomena.

Different test samples of masks are prepared and are worn on the manikin head, and model-cough impingement studies have been conducted. The penetrated daughter droplets in manikin experiments for the samples A and C have been shown in Fig. 5. Figures 5(b)–5(g) show the ejected daughter droplets after penetration through different types of masks (in decreasing order of the penetration volume percentage) (see Table IV). The layer A that has a relatively larger pore size ($\epsilon \sim 45 \mu\text{m}$) and porosity ($\phi \sim 17\%$) results in a considerable amount of large-sized droplets along with aerosolization; see Fig. 5(b). The samples, layer C and $2 \times$ layer A, have similar pore size ($\epsilon \sim 30 \mu\text{m}$) and porosity ($\phi \sim 5\%$); however, the latter exhibited significantly fewer penetrated droplets due to its higher fabric thickness compared to the former, as shown in Figs. 5(c) and 5(d). It is also interesting to observe that the cone angle of the penetrated daughter droplet spray has increased to $\sim 60^\circ$ while using layer A and $\sim 80^\circ$ for layer C and $2 \times$ layer A samples. This shows that the forward momentum of the

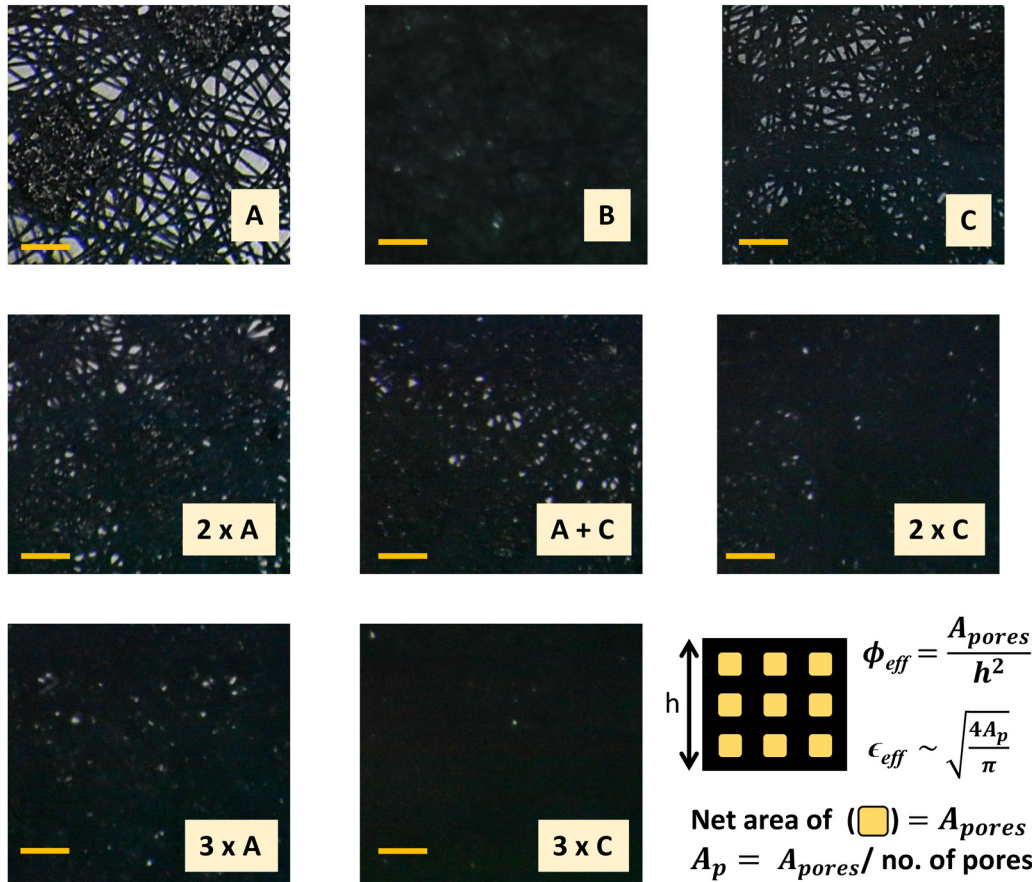


FIG. 3. Magnified cross-sectional images (shadowgraphy) of each of the test samples as given in Table I. The samples are layers A, B, C (single-layer samples), 2 × A, A + C, 2 × C (double-layer samples), and 3 × A, 3 × C (triple-layer samples). All scale bars represent 300 μm. The methodology for obtaining pore size and porosity is shown in the bottom-right corner.

impinging jet has been dissipated and distributed due to the presence of the mask. This effect is minimal in the case of layer A sample, which exhibited a relatively smaller cone angle due to its larger porosity, thus resulting in relatively low viscous dissipation. Figure 5(e) corresponds to the sample, which is the combination of layer A and layer C. It exhibited significantly reduced penetration volume compared to the

TABLE I. The characteristics of different mask samples and their combinations in multilayer configuration.

Sl No.	Samples	Porosity (ϕ)%	Pore size, ε (μm)	Thickness, t _m (μm)
1	Layer A	17.22 ± 2.72	45.20 ± 3.64	430.11 ± 12.57
2	Layer B	0.14 ± 0.01	22.20 ± 0.79	595.26 ± 13.96
3	Layer C	4.84 ± 0.78	31.68 ± 1.08	512.7 ± 12.19
4	2 × layer A	5.23 ± 0.77	31.51 ± 1.04	873.42 ± 11.76
5	Layer A + C	1.95 ± 0.31	25.90 ± 0.89	950.39 ± 11.15
6	2 × layer C	0.33 ± 0.02	23.40 ± 0.72	1086.21 ± 13.46
7	3 × layer A	0.39 ± 0.09	24.03 ± 0.84	1285.3 ± 15.66
8	3 × layer C	0.04 ± 0.01	28.44 ± 0.61	1546.95 ± 11.28

2 × layer A sample because of the presence of less porous layer C (ϕ ~ 5%) along with layer A sample. Figures 5(f) and 5(g), the two samples 2 × C and 3 × A, having very low porosity (ϕ ~ 0.3%) exhibit almost negligible amount of penetrated daughter droplets all of which are totally in the aerosolization range.

In this section, first, the droplet penetration mechanism has been explored for different sizes of impinging droplets. Then, multi-step penetration criteria based on droplet velocity and mask properties have been given, which estimate the penetration possibility of a spray with good accuracy. Further, the effect of different mask properties on the penetrated volume percentage, droplet size, and velocity distribution has been investigated. Additional experiments were performed to check the effectiveness of the mask worn by a susceptible person in the proximity. Finally, the virus filtration efficacy of the mask has been investigated by using virus-emulating nanoparticle-laden surrogate respiratory droplets to check for the nanoparticle entrapment in the mask.

A. Droplet penetration mechanism

The impinging cough droplets consist of both larger- and smaller-sized droplets with a velocity scale of 10 m/s. The spray consists of a significant number of smaller-sized droplets in the aerosol

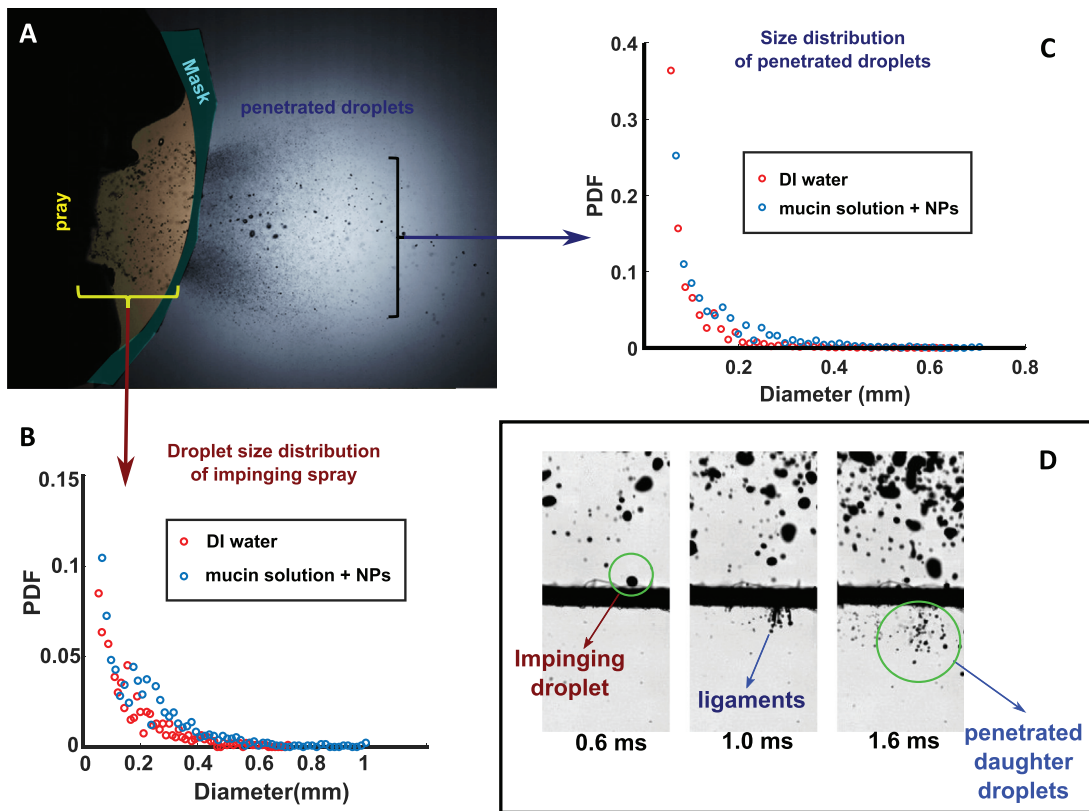


FIG. 4. (a) The schematic of shadowgraphy image of spray droplets ejected from the nozzle orifice (located in the mouth of manikin): before and after penetration through the mask. (b) The size distribution of impinging spray using DI water and surrogate respiratory fluid [mucin solution + 10^6 nanoparticles (NP) per ml], (c) a sample comparison of the size distribution of penetrated droplets for DI water and surrogate respiratory fluid (mucin solution + 10^6 NP particles per ml) through a mask sample (layer A), and (d) the zoomed-in view depicting the penetration mechanism of droplets leading to ligament formation and secondary atomization.

range ($<100 \mu\text{m}$), along with a fewer number of larger-sized droplets ($>250 \mu\text{m}$). However, the larger cough droplets contribute to more than 94% of the total volume⁸ and hence can potentially carry more viral loading.³⁵ Thus, blocking these larger-sized droplets is the primary purpose of the mask. Moreover, the impinging cough droplets atomize into aerosolization range ($<100 \mu\text{m}$) after penetrating through the mask, which can remain airborne for longer periods and can contribute to infection spread.^{8,9} Hence, this atomization aspect also needs to be investigated by studying the penetration mechanism of the droplets through the mask fabric.

The fate of the individual droplets in the impinging spray after the impact depends on the droplet size, velocity, and the mask properties. The droplet impingement on a porous surface like mask fabric involves three different phenomena.²⁹ The liquid passes through the fabric pores and extrudes out on the other side in the form of ligaments. These ligaments break up due to Rayleigh–Plateau instability and result in the formation of daughter droplets. Some portion of the initial droplet spreads along the fabric surface, and bounce-back occurs. The remaining volume of the droplet is retained in the fabric through absorption and percolation. As the droplet impinges on the mask fabric, the initial kinetic energy of the impinging droplet is lost to different events such as viscous dissipation, overcoming surface tension, and spreading of liquid along the fabric surface. The remaining

available energy is converted into the kinetic energy of the ligaments that extrude through the fabric pores. This available kinetic energy dictates the ligament length and velocity of the daughter droplets after the ligament breakup. The size and velocity of the ligaments also affect the size of the daughter droplets.

The droplet penetration involved in the spray impingement, characterized by multiple droplet sizes, velocity scales, and the dependency of penetration on droplet diameter needs to be investigated. The time-series images of spray impingement and penetration for sample A have been shown in Fig. 6. The process of formation of ligaments due to extrusion of droplets through the pores can be observed in Fig. 6(a) (time-series images) for different impinging droplet diameters. The time-series images clearly show the process of atomization of spray droplets into smaller size (aerosol range) at high impingement velocity. The zoomed-in version of larger droplet impingement in the spray ($\sim 500 \mu\text{m}$) has been shown in Fig. 6(b), which clearly shows the formation of ligaments and ligament breakup phenomenon. The Rayleigh–Plateau instability²⁹ causes this ligament breakup event and forms daughter droplets having a lower diameter range, depending on the pore size and ligament velocity. Furthermore, the zoomed-in images of the impingement of smaller droplets ($\sim 100 \mu\text{m}$) are shown in Fig. 6(c), which shows the penetration of smaller droplets as well, given that they have sufficient kinetic energy. These small droplets

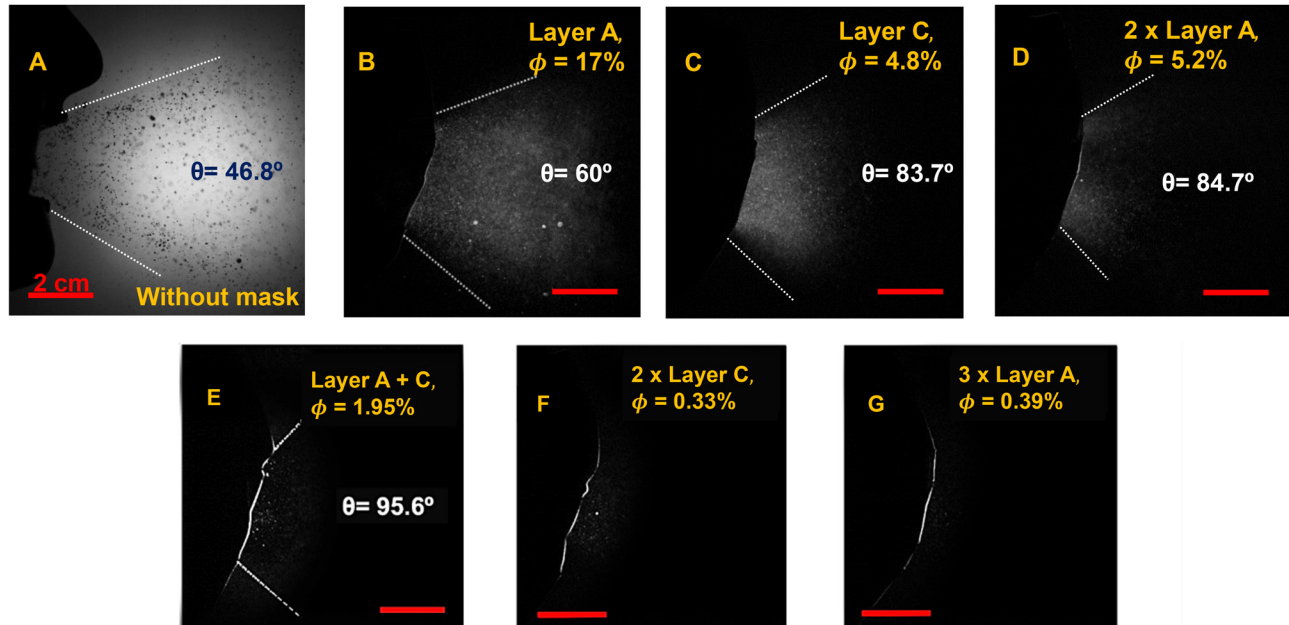


FIG. 5. Spray characteristics and the experimental images of spray impingement using a manikin with and without mask. (a) Shadowgraphy image of model-cough generated using spray nozzle in a manikin without mask, (b)–(g) enhanced high-speed images (inverted) of penetrated daughter droplets with different mask samples (in decreasing order of penetration volume percentage): (b) layer A, (c) layer C, (d) 2 × layer A, (e) layer A + C, (f) 2 × layer C, (g) 3 × layer A. The values of porosity (ϕ) for each sample, as well as the cone angle of the spray ejected into surroundings for the respective samples, are shown. All the scale bars represent 2 cm. Multimedia view: <https://doi.org/10.1063/5.0093297.1>

(with diameter larger than pore size) undergo atomization into further smaller-sized daughter droplets through ligament formation. Hence, it can be inferred that both larger and smaller droplets in the cough can potentially lead to aerosolization and contribute to the volume penetrated. The smaller-sized droplets get atomized into even smaller droplets leading to a higher extent of aerosolization.

B. Droplet penetration criteria

1. Two-step penetration criteria

The penetration dynamics of the droplets also depend upon the mask properties like porosity (ϕ), pore size (ϵ), and thickness (t_m). Thus, penetration criteria have to be developed for determining whether the penetration of the droplets occurs through the pores of a given mask sample or not. Following similar lines as in our previous studies and the literature,^{29,30} the main physical mechanisms that oppose or resist the penetration of droplets through the mask are viscous dissipation along the thickness and capillary forces due to surface tension at the pore level.

Hence, the penetration criteria have to consider both the opposing effects, that is, one with respect to viscous dissipation and other with respect to surface tension effects (Weber number, We_ϵ). Since both these effects oppose the penetration of droplets, the momentum in the impinging droplets has to overpower both capillary and viscous dissipation effects for the penetration to be possible. Hence, two-step criteria are considered based on capillary effects and viscous dissipation, both of which have to be followed for penetration to occur. Sahu *et al.*²⁷ reported that beyond a threshold impact velocity, irrespective

of hydrophobicity and initial mass, the liquid penetration always occurs through a porous network of fibers. The liquid passes through the pores of the fabric in the form of ligaments, extruding outward from the pores. For a fabric pore size of ϵ and thickness t_m , the liquid ligaments can pass through the pores when the kinetic energy (E_k) exceeds the viscous dissipation (E_d) in the pores.²⁷ Penetration criteria have been formulated using this argument based on viscous dissipation as given below:

$$E_k \sim \left[\rho d^3 \left(\frac{Vd}{\epsilon} \right)^2 \right] \gg E_d \sim \left[\frac{\mu}{\epsilon} \left(\frac{Vd}{\epsilon} \right) d \epsilon \left(\frac{d}{\epsilon} \right)^3 t_m \right], \quad (1)$$

$$Re_\epsilon \left(\frac{\epsilon}{t_m} \right) \gg 1. \quad (2)$$

This suggests that penetration only occurs when the condition $Re_\epsilon \left(\frac{\epsilon}{t_m} \right) \gg 1$ is followed.

The second penetration criterion is based on the surface tension effects, which suggest that droplet penetration can only occur when the dynamic pressure ($\sim \rho V^2$) exerted by the impinging droplet exceeds the capillary pressure ($\sim 4\sigma/\epsilon$) inside the fabric pores.^{29,53} Hence, according to the surface tension criterion, penetration only occurs when

$$\rho V^2 > 4\sigma/\epsilon, \quad (3)$$

$$\rho V^2 \frac{\epsilon}{4\sigma} > 1, \quad (4)$$

$$We_\epsilon > 1, \quad (5)$$

where ρ is liquid density, σ is the surface tension between the water–air interface, V is impact velocity, ϵ is pore size, and We is Weber number.

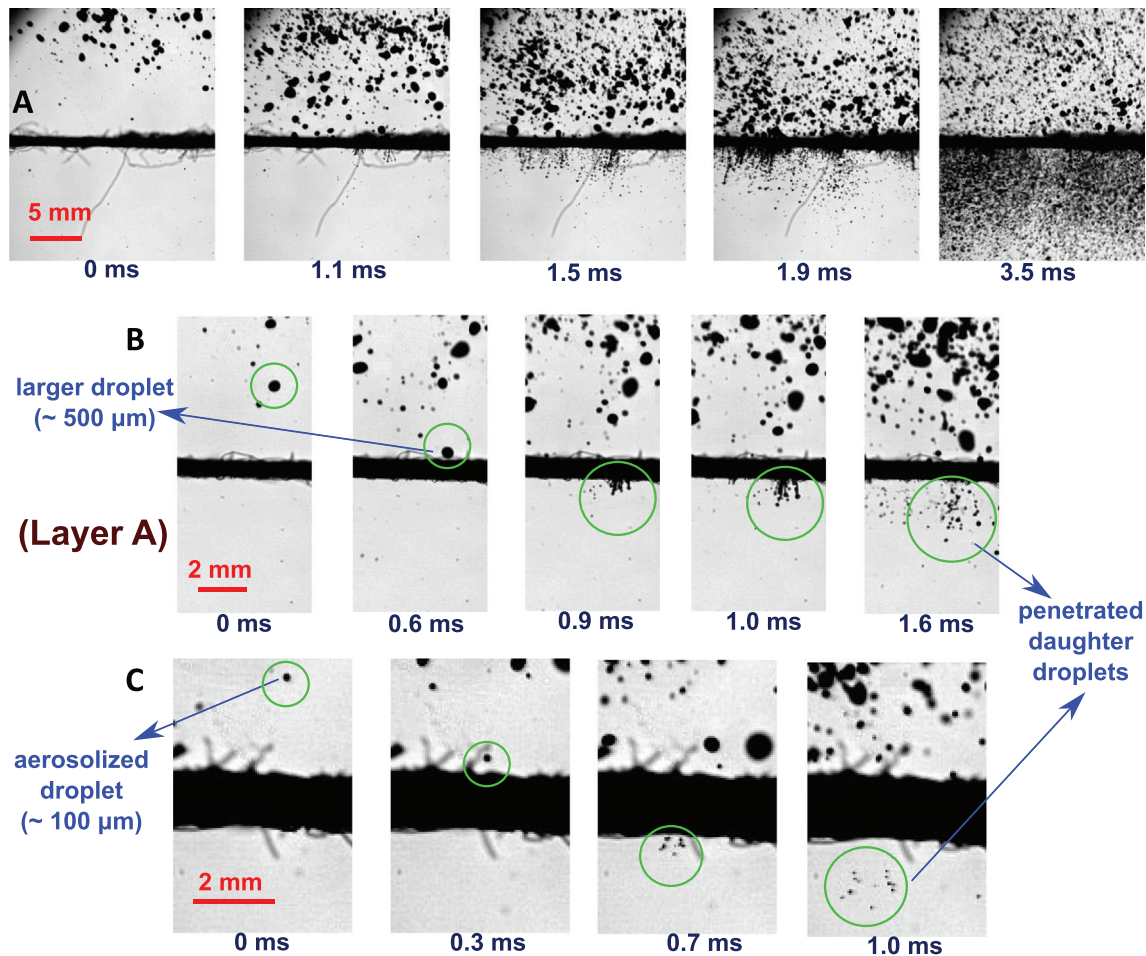


FIG. 6. (a) The time-series images of the spray impingement on a mask sample (layer A). (b) Zoomed-in time-series images of impingement of larger-sized droplet ($\sim 500 \mu\text{m}$) in the impinging spray (for sample A), (c) zoomed-in time-series images of impingement of aerosolized smaller-sized droplet ($\sim 100 \mu\text{m}$) in the impinging spray (for sample A). All the scale bars are represented in the images.

These two criteria do not contain any droplet diameter-dependent term and are only dependent on the mask fabric properties. However, it is to be noted that these criteria are derived under the assumption of $d > \epsilon$ and will not be valid for $d < \epsilon$ cases. Additionally, it is evident from Eqs. (2) and (5) that the two mask properties ϵ and t_m affect the two penetration criteria differently. Pore size (ϵ) affects both viscous dissipation and surface tension criterion; however, thickness (t_m) only affects the viscous dissipation criterion. Higher the value of t_m , the parameter for viscous dissipation criterion will be lower, suggesting higher viscous dissipation. From this, the relative importance of the two criteria in the case of a mask sample with specific properties can be known by the ratio of t_m and ϵ . The higher value of the ratio t_m/ϵ for a given mask sample suggests that the viscous dissipation criterion is more dominant and relevant in determining the possibility of droplet penetration [see Eq. (2)]. Considering the maximum value of velocity ($\sim 14 \text{ m/s}$) associated with the impinging spray in current experiments, the value of parameters of the two criteria and the ratio t_m/ϵ for all the different test samples have been shown in Table II. It is to be noted that the penetration phenomenon

fundamentally occurs at the local pore level. Hence, only the local properties of the mask like pore size (ϵ) and thickness (t_m) are considered for the penetration criteria but not porosity (ϕ), which is a global parameter and does not affect pore-level dynamics.

From Table II, it can be observed that the t_m/ϵ ratio is of order $O(10)$ for all the cases, suggesting that the viscous dissipation criterion should be more relevant for these mask samples. This matches with the observation of Krishan *et al.* showing that the t_m/ϵ ratio is of order $O(10)$ in the case of surgical mask, which are used in the current study.²⁹ This is reflected in the surface tension criterion parameter values, that is, for all the samples, $We_\epsilon > 15$ (far away from the criterion, i.e., $We_\epsilon > 1$), which suggests that the capillary pressure is overpowered by the dynamic pressure of impinging droplets in all the cases, making the surface tension effects negligible. This suggests that viscous dissipation is the only other resisting or opposing effect that can impede the penetration. This necessitates the reliance on viscous dissipation criterion as well, since the surface tension criterion alone is insufficient to estimate the penetration characteristics of the spray impingement. Using viscous dissipation criterion, the value of the

TABLE II. Table shows the two penetration criteria for different mask samples calculated at maximum value of impingement velocity (~ 14 m/s). The values of porosity (ϕ), pore size (ϵ), thickness (t_m), and t_m/ϵ ratio are also tabulated corresponding to the respective samples. The two penetration criteria are based on viscous dissipation: $Re_\epsilon(\frac{\epsilon}{t_m}) \gg 1$, and surface tension: $We_\epsilon > 1$. Green color fill indicates that penetration does not occur, and orange color fill indicates that penetration occurs, for those samples experimentally. Based on the corresponding criterion, red font indicates that penetration is possible and green font indicates that penetration is not possible, for that particular sample.

	$\phi\%$	ϵ (μm)	t_m (μm)	$Re_\epsilon(\frac{\epsilon}{t_m})$	t_m/ϵ	We_ϵ
Layer A	17.22	45.2	430	77.96	9.51	30.76
Layer C	4.84	31.68	513	32.10	16.19	21.56
2 \times layer A	5.23	31.51	873	18.66	27.70	21.44
Layer A + C	1.95	25.9	950	11.58	36.67	17.63
2 \times layer C	0.33	23.4	1086	8.27	46.41	15.93
3 \times layer A	0.39	24.03	1285	7.37	53.47	16.35
Layer B	0.14	22.2	595	13.59	26.80	15.11
3 \times layer C	0.04	28.44	1547	8.58	54.39	19.36

parameter $[Re_\epsilon(\epsilon/t_m)]$ is found to be of order $O(1)$ for the samples 2 \times C, 3 \times A, and 3 \times C, and its value is $\gg 1$, that is, $O(10)$ for all the other samples. This suggests that according to the viscous dissipation criterion, penetration should not occur in the case of the three samples 2 \times C, 3 \times A, and 3 \times C. However, from the experiments, the penetration is not observed only for the two samples B and 3 \times C samples, and very low penetration is observed in the case of sample 3 \times A. Hence, we can conclude that the viscous dissipation criterion is relatively in good agreement with the experiments in predicting the absence of penetration with a minor discrepancy in the case of the sample 3 \times A. However, experimentally sample B does not exhibit penetration as well, which is not included by the viscous dissipation criterion based on the local parameters. The local pore-level two-step criteria as discussed in this section predict droplet penetration only when the droplet size (d) is comparable to pore size (ϵ) and will not be valid for $d < \epsilon$ cases (where droplet-pore interaction is not significant). The two-step criteria are able to predict the penetration possibility correctly for all the samples except one, which is reasonable. This is because it is only applicable fully for single-droplet impingement for $d > \epsilon$ and may not be entirely sufficient for the spray impingement phenomenon.

2. Additional penetration criteria for spray impingement

These two criteria based on viscous dissipation and surface tension focus only on the penetration characteristics locally at the pore level, which is the possible reason for this discrepancy. Since the current experiments involve spray impingement, the two-step criteria do not give a full picture of the penetration phenomena, as the spray is not localized at an individual pore. In the case of a spray, even though the local mask properties allow the penetration to occur, the penetration may not always ensue as the individual droplets might not always encounter the gaps or pores in their path to pass through. Since these criteria are focusing on local pore-level penetration, they may not be sufficient to predict the extent of penetration for spray impingement

with a global outlook, without considering the global parameters. Hence, in addition to the pore-level two-step criteria, a global property has to be considered in the scaling, especially in order to estimate the penetration for sprays.

Porosity (ϕ) is one such property of mask, which is the proportion of total amount of space or gap available for droplets to penetrate through, and it is not local pore-level property. In order to get a global penetration criterion, both global parameters corresponding to mask as well as the impinging spray are needed to be scaled together. Porosity (ϕ) can be considered as one of the parameters for global mask property, and there is a necessity for the formulation of a global spray parameter that is analogous to porosity. Since the porosity is the cross-sectional areal ratio of available gaps to the total area, a cross-sectional areal quantity has to be scaled for the impinging spray. Hence, a new spray parameter is formulated called cross-sectional spray areal density (\mathbb{C}), which is the proportion of the total cross-sectional projected area of spray droplets ($A_{\text{spray } c/s}$) with respect to the available area of the mask at any given instant, near the point of impact.

The side-view shadowgraphy images are used to estimate the parameter \mathbb{C} , due to the experimental limitations to accurately capture the cross-sectional view of the droplets in the impinging spray. As shown in Fig. 7, the droplets present at the vicinity of the mask surface just before the impact are considered and their individual horizontal width is used for the calculation of projected area for each of the droplet, assuming axisymmetry. The corresponding cross-sectional projected area summed over all the droplets that are located just above the mask is used to calculate the total cross-sectional projected area of the spray ($A_{\text{spray } c/s}$). This value is averaged over multiple frames and multiple experimental runs, in the window of consideration to get the final value of $A_{\text{spray } c/s}$. The ratio of $A_{\text{spray } c/s}$ and total mask cross-sectional area ($A_{\text{mask}} \sim h^2$) gives the parameter \mathbb{C} (cross-sectional spray areal density), whose value is found to be $(1.58 \pm 0.3)\%$ from the experimental data. The same averaged value of \mathbb{C} is used for all the cases for simplicity, since the valve opening time and upstream pressure were maintained same for generating the spray in all the experimental runs for all the cases. Finally, for formulating the third penetration criterion for spray, the ratio of the two global parameters based on the mask (ϕ) and spray (\mathbb{C}) properties is considered, given as

$$\frac{\phi}{\mathbb{C}} = \frac{A_{\text{pores}}/A_{\text{mask}}}{A_{\text{spray } c/s}/A_{\text{mask}}} = \frac{A_{\text{pores}}}{A_{\text{spray } c/s}}. \tag{6}$$

The ratio ϕ/\mathbb{C} represents the amount of pore area available per unit spray cross-sectional area. This gives a qualitative measure of the probability of penetration of the spray. The lower value of ϕ/\mathbb{C} leads to a lesser probability of spray penetration. Hence, for $\frac{\phi}{\mathbb{C}} \ll 1$, the probability of spray penetration is very low, leading to significantly low penetration volumes.

The discrepancy observed in the case of two-step criteria is because the criteria do not account for the porosity of the sample (ϕ). Sample B shows no penetration experimentally, but the two-step criteria predicted penetration is possible in this sample. However, the significantly low value of porosity for this sample B ($\phi \sim 0.14$) results in restricting the penetration, even though penetration should be theoretically possible at the pore level as the initial kinetic energy can surpass both viscous dissipation and capillary effects. This effect is incorporated using the ratio ϕ/\mathbb{C} (shown in Table III) where the two

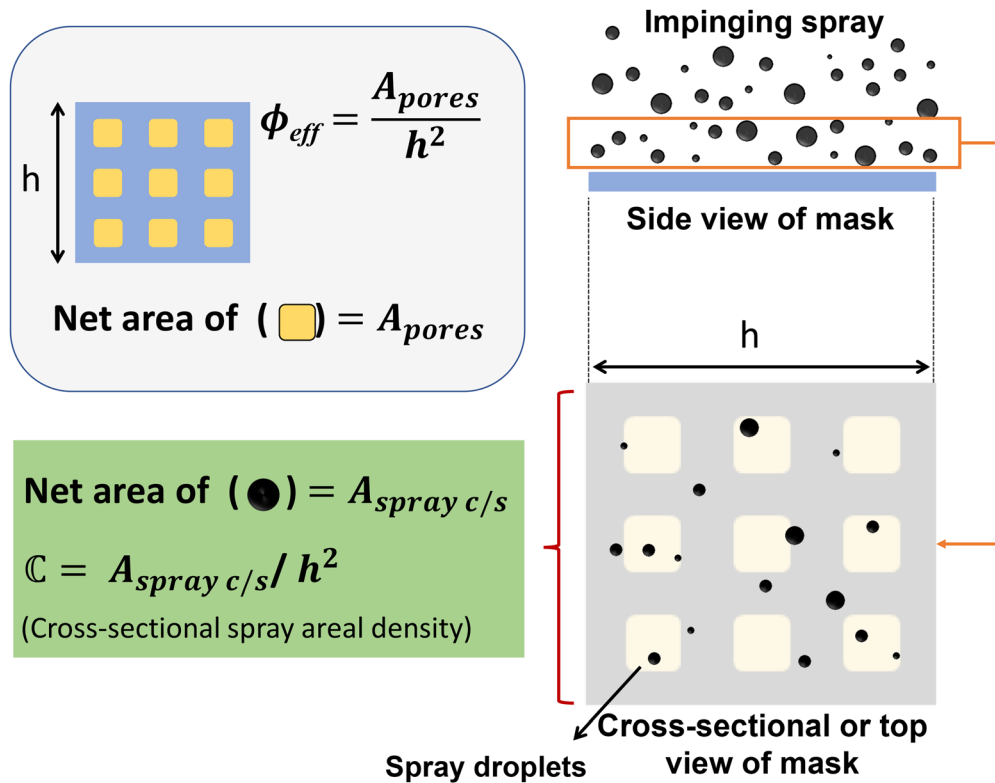


FIG. 7. The methodology of calculation of the parameter \mathbb{C} (cross-sectional spray areal density) from experimental data. The spray droplets just before their impact on the mask (enclosed by orange box) are considered for the calculation of \mathbb{C} . Calculation of porosity is given in the top left.

samples **B** and $3 \times \mathbf{C}$ exhibit no penetration experimentally, as they have a significantly low value of ratio ϕ/\mathbb{C} , of the order $\leq O(0.1)$, as shown in [Table III](#). Hence, we can conclude that penetration will not occur for $\frac{\phi}{\mathbb{C}} \ll 1$ based on this third penetration criteria and is in good agreement with the experiments. This new criterion also explains why a small amount of penetration is possible in the case of sample $2 \times \mathbf{C}$ due to its relatively higher porosity, even though the two-step criteria indicated no penetration.

TABLE III. The table shows the values of the ratio ϕ/\mathbb{C} in the decreasing order of the corresponding porosity (ϕ) for different samples giving a qualitative estimate for penetration probability for spray impingement. The green fill represents no penetration, and orange fill indicates the occurrence of penetration for the respective sample.

	Porosity (ϕ)%	$\frac{\phi}{\mathbb{C}}$
Layer A	17.22	10.90 ± 2.8
$2 \times$ layer A	5.23	3.31 ± 0.78
Layer C	4.84	3.06 ± 0.62
Layer A + C	1.95	1.23 ± 0.30
$3 \times$ layer A	0.39	0.25 ± 0.06
$2 \times$ layer C	0.33	0.21 ± 0.05
Layer B	0.14	0.09 ± 0.02
$3 \times$ layer C	0.04	0.03 ± 0.006

Additionally, from [Table III](#) it can be observed that the values of the ratio $\frac{\phi}{\mathbb{C}} > 1$ for the samples **A**, **C**, **A + C**, and $2 \times \mathbf{A}$ suggest a higher probability of spray penetration and it agrees with the experiments. For the other samples in the range of $O(0.1) < \frac{\phi}{\mathbb{C}} < O(1)$, that is, **A + C**, $3 \times \mathbf{A}$, and $2 \times \mathbf{B}$, the penetration is significantly lower due to the lower value of the ratio ϕ/\mathbb{C} . This newly defined ratio ϕ/\mathbb{C} gives an estimate of the extent of penetration and penetration possibility of the impinging spray on a mask surface (at the global level). This new criterion also considers the smaller $d < \epsilon$ droplets unlike the two-step criteria, as it has been formulated based on global parameters instead of local level droplet–pore interaction. Hence, the third criterion can compensate for the $d < \epsilon$ droplet range for which the two-step criteria are invalid. Thus, the combination of both two-step criterion and ϕ/\mathbb{C} ratio criterion can give accurate penetration criteria for the spray impingement on a mask fabric, which agrees well with the experimental observations.

It has been shown by Smith *et al.* that the aerosol transmission mode is a less efficient route of transmission in the case of asymptomatic or mildly symptomatic people. Nevertheless, the aerosol transmission was shown to contribute significantly to the spread of COVID-19, especially under low ventilation.⁵⁴ Hence, the aerosol ($< 20 \mu\text{m}$) filtration of the mask also needs to be estimated. However, since aerosol filtration is not purely hydrodynamic in nature,⁴⁹ it is outside the scope of the current study. Nevertheless, it is to be noted that the two-step droplet penetration criteria in this study are formulated by considering the hydrodynamic aspects alone and are not applicable for impinging

TABLE IV. Table shows the different samples in decreasing order of the penetration volume percentage in spray impingement experiments. The values of porosity (ϕ), pore size (ϵ), thickness (t_m), and t_m/ϵ ratio are also tabulated corresponding to the respective samples. The penetration volume percentage generally follows a decreasing trend with the porosity. Blue color fill indicates the samples for which percentage volume penetrated deviates from this trend. The red font indicates the lower penetration volume percentage in the deviating samples due to higher thickness. This effect of t_m is attributed to higher t_m/ϵ ratio indicating the dominance of viscous dissipation effects. Green fill indicates no penetration, and the orange fill indicates the occurrence of penetration for the respective sample.

	$\phi\%$	ϵ (μm)	t_m (μm)	t_m/ϵ	% volume penetrated
Layer A	17.22	45.2	430	9.51	16.67
Layer C	4.84	31.68	513	16.19	4.55
2 \times layer A	5.23	31.51	873	27.70	0.85
Layer A + C	1.95	25.9	950	36.67	0.38
2 \times layer C	0.33	23.4	1086	46.41	0.34
3 \times layer A	0.39	24.03	1285	53.47	0.20
Layer B	0.14	22.2	595	26.80	0.00
3 \times layer C	0.04	28.44	1547	54.39	0.00

aerosol. Moreover, since the third criterion of ϕ/C ratio is formulated purely based on the geometry, it can qualitatively give the probability of the spatial interaction of aerosol particles with the mask fibers. It is a general understanding that when the aerosol particles interact with a filter fiber, they get collected by the fiber and are retained through van der Waals forces.⁵⁵ Thus, the lower value of ϕ/C ratio can roughly be correlated with higher aerosol filtration efficiency.

C. Penetrated volume percentage

The percentage volume penetrated during the spray impingement has been shown in Table IV. The percentage volume penetrated is calculated from the shadowgraphy experiments, and the calculated values are in good agreement with the microbalance measurements of the penetrated spray for different cases with the uncertainty of less than $\pm 10\%$. The pore size (ϵ) of all the samples is in a similar range, and their values are in the same order of O (10), because of which ϵ does not have a significant effect on the percentage volume penetrated. However, the porosity (ϕ) affects the volume penetration percentage because the net gap available for the liquid to pass through directly affects the volume penetrated.

Additionally, a general trend is observed where the percentage of volume penetrated decreases with decrease in porosity (ϕ); however, there are some exceptions to this general trend. In the case of the samples C and 2 \times A, the porosity increases slightly from samples C to 2 \times A, but the percentage volume penetrated decreased drastically. This is because of the effect of significantly higher fabric thickness (t_m) in sample 2 \times A compared to sample C and both the samples having the porosity (ϕ) and pore size (ϵ) in a relatively similar range. The higher value of fiber thickness (t_m) contributes to higher viscous dissipation, which leads to lower penetrated volume percentage in sample 2 \times A compared to C. In the case of the samples 2 \times C and 3 \times A, similar to the previous case, the porosity (ϕ) and pore size (ϵ) are in the similar range; however, fabric thickness (t_m) is relatively higher in the case of 3 \times A. Moreover, the effect of the increase in fabric thickness (t_m) is

more compared to the effect of the increment in porosity (ϕ) or pore size (ϵ), which caused the net decrease in percentage volume penetrated from sample 2 \times C to sample 3 \times A. The dominant effect of the fabric thickness (t_m) on penetration volume can be attributed to the higher value of t_m/ϵ , suggesting the dominance of viscous dissipation effects in these samples as mentioned in the previous section. Except for the samples B and 3 \times C, all the other samples exhibited penetration. Another interesting observation is that the penetration volume percentage has a weak positive correlation with the ϕ/C ratio, because of the porosity variation. It is to be noted that the ϕ/C ratio gives a decent estimate of penetration of the spray. For $\phi/C < 1$, all the samples have a significantly low penetration volume percentage ($< 0.4\%$) suggesting that ϕ/C ratio is decently effective in giving a rough estimate of the extent of penetration. Additionally, the ϕ/C ratio accurately predicts the possibility of penetration in the samples in which the local mask properties allow penetration but the global property (ϕ) may or may not always allow the penetration depending on the impinging spray density, which is incorporated in ϕ/C ratio. The two-step criteria give insight into the possibility of penetration; however, in the case of spray impingement the complete picture is only obtained when it is combined with ϕ/C ratio. The general trend of penetration volume percentage is given by ϕ/C ratio.

D. Droplet size and velocity distribution

The model-cough used in the experiments (as shown in Sec. II) replicates similar velocity and size distribution characteristics of an actual cough, as shown in Figs. 8(b) and 8(c). It is to be noted that all the PDFs (probability distribution) plotted in Fig. 8 are normalized before plotting. Figures 8(d)–8(f) show the PDFs of the penetrated droplet velocity distribution for different samples, which follow the bell-shaped trend. Figures 8(d) and 8(f) depict the effect of the addition of multiple layers to the incident spray. In both the cases, the velocity PDF curve is observed to shift toward left with the addition of each extra layer. This suggests that each additional layer contributes to the dissipation of initial kinetic energy of the impinging spray. It is also to be noted that the ratio t_m/ϵ increases drastically from ~ 10 to ~ 53 with addition of two more layers in the case of sample A (similarly for sample C, see Table IV), suggesting increased viscous dissipation effects. This can be attributed to both increased viscous dissipation due to higher net fabric thickness and reduced effective porosity due to additional layers [see Fig. 8(d), multimedia view]. The value of the peak is also observed to increase with additional layers suggesting more droplets get decelerated to lower values of velocity. Figure 8(e) (multimedia view) shows the effect of the combination of mask layers with a different porosity. The layer A and layer C individually have porosities $\phi \sim 17\%$ and 5% , allowing $\sim 16\%$ and 4.5% of volume to penetrate through them, respectively. The combination of these two layers shifts the curve to the left significantly because of the low porosity of the layer C contributing to a higher level of viscous dissipation in addition to the effect of added fabric thickness [see Fig. 8(e)].

In all cases, the velocity range of penetrated droplets is in the range of 0–2 m/s, suggesting a physical obstruction like a mask can decelerate the high velocity (~ 10 –14 m/s) cough droplets to the order of < 2 m/s. However, having better mask properties such as lower porosity and pore size or higher thickness leads to a higher proportion of droplets that are decelerated to lower velocities (< 1 m/s).

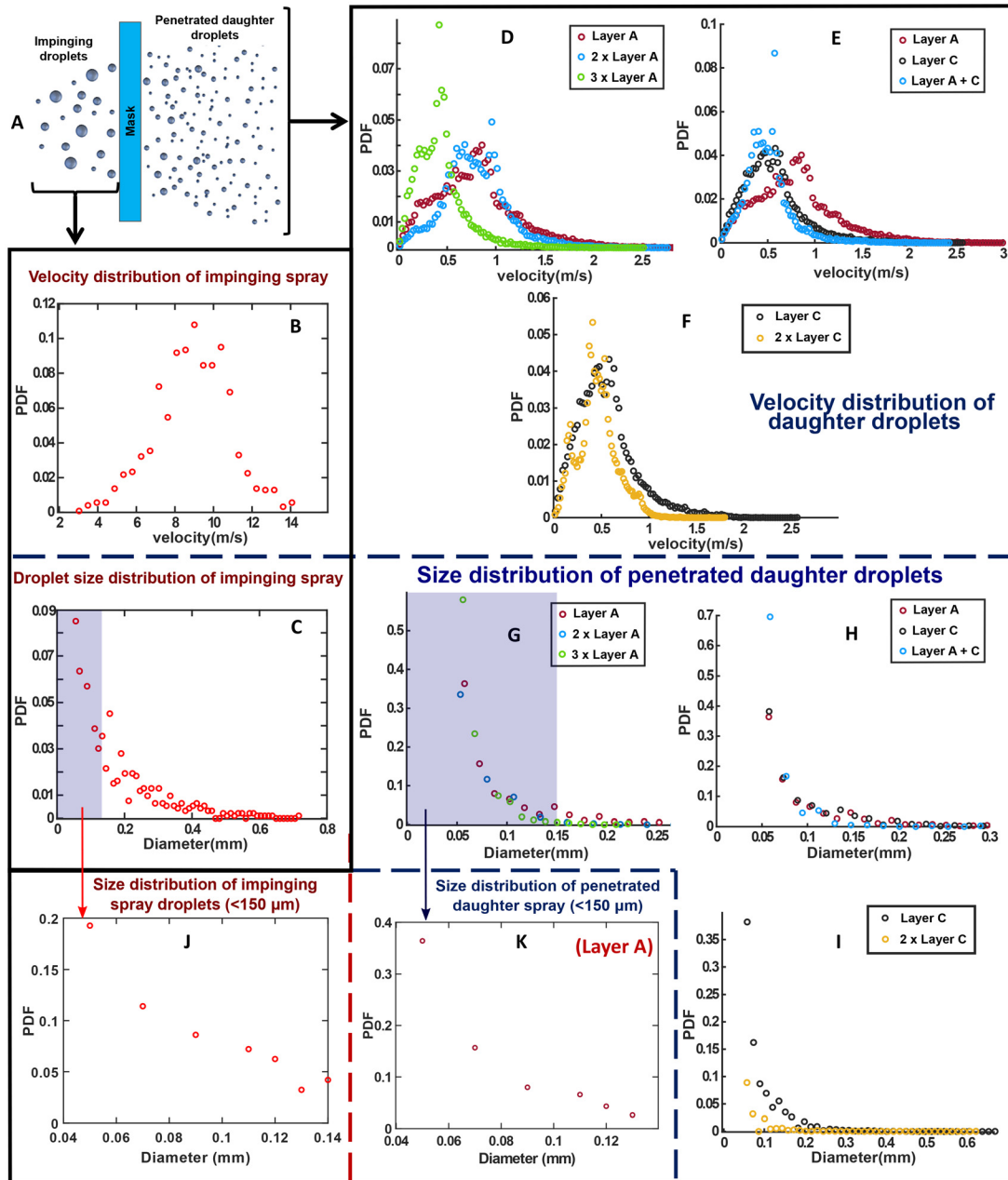


FIG. 8. The spray characteristics of spray impingement on mask surface. (a) The schematic depiction of spray impingement and penetration of daughter droplets through a mask, (b) velocity distribution (PDF) for the impinging spray droplets, (c) droplet diameter distribution (PDF) for the impinging spray, (d)–(f) velocity distribution (PDF) for the penetrated daughter droplets for different samples: (d) layer A, 2 × layer A, and 3 × layer A, showing effect of number of layers, (e) layer A, layer C, and layer A + C, showing the effect of combination of different samples, (f) layer C and 2 × layer C, (g)–(i) droplet size distribution (PDF) for the penetrated daughter droplets for different samples: (g) layer A, 2 × layer A, and 3 × layer A, (h) layer A, layer C, and layer A + C, (i) layer C and 2 × layer C, (j) and (k) droplet size distribution (PDF) in aerosolization range (<150 μm). (j) For the impinging droplets on the mask, (k) for the penetrated daughter droplets for sample A. Multimedia views: <https://doi.org/10.1063/5.0093297.2>; <https://doi.org/10.1063/5.0093297.3>; <https://doi.org/10.1063/5.0093297.4>

This extent of deceleration of the impinging cough droplets is essential to contain the spread of these pathogen-loaded droplets from an infected person. However, the droplets in the aerosolization range can remain suspended in air for longer durations and can be

transferred to different locations by the air flow, which is another important issue.

Figures 8(g)–8(i) show the PDFs of the droplet size distribution after penetration through the corresponding mask samples. The

diameter of the penetrated daughter droplets depends on the ligament size and velocity, which is governed by the mask pore size (ϵ) and fabric thickness (t_m).²⁹ The pore size contributes to capillary effects and viscous dissipation, whereas fabric thickness affects only viscous dissipation. In the case of Fig. 8(g), addition of an extra layer for the sample layer A leads to decrease in effective pore size and increase in fabric thickness. The increase in fabric thickness reduces the ligament velocity and shorter ligaments due to viscous dissipation. Additionally, the decrease in pore size leads to the formation of smaller daughter droplets after ligament breakup. This is reflected in Fig. 8(g), where the probability decreases for the formation of larger droplets and increases for the formation of smaller droplets due to the additional layer [see Fig. 8(d)]. Similar behavior is observed in the case of layer C [see Fig. 8(i)]. Additionally, the curve shifts significantly to the left in the case of layer C, which can be attributed to the lower pore size and higher thickness of layer C. In the case of Fig. 8(h), the similar trend is observed where with the combination of the samples A and C, the PDF curve shifts to the left, and height of the curve, which is present in the lower diameter range increases. Hence, the probability of the formation of smaller droplets increases. The size distribution has been plotted for droplets belonging to the aerosolization range ($< 150 \mu\text{m}$) for impinging droplets and penetrated droplets in Figs. 8(j) and 8(k), respectively. These plots give insight into the aerosolization occurring due to ligament breakup of smaller droplets. The probability of smaller-sized droplets is observed to be higher for the daughter droplets after penetration in the aerosolization range [see Fig. 8(k)]. This is because even smaller droplets contribute to aerosolization, as shown in Fig. 6(c).

It is to be noted that in all the droplet size distribution PDFs shown, due to the experimental limitations involved in imaging the spray, the minimum droplet diameter that can be measured with decent accuracy is $50 \pm 23.8 \mu\text{m}$. Hence, the droplet diameter PDFs do not have any data points below the diameter value of 0.05 mm, which forms the left portion of the bell-curve trend for penetrated daughter droplet diameter PDF. The PDFs of the samples layer B and $3 \times$ layer C are not plotted as the penetration is not detected in these samples.

Comparing the two samples layer A and layer C, the pore size of sample A is larger compared to sample C, which tends to the formation of thicker ligaments in the sample A leading to larger-sized daughter droplets [see the supplementary material Figs. S2(a) and S2(d)]. However, the fabric thickness of sample A is significantly lower, which tends to increase the ligament velocity and hence enhance the ligament breakup phenomenon. Additionally, the PDFs of sample A and sample C look similar with similar type of droplet distribution having a peak at around $60\text{--}70 \mu\text{m}$. Hence, it can be inferred that these two effects of pore size and fabric thickness counteract each other in influencing the droplet size distribution in these two samples, comparatively [see Figs. 8(g) and 8(I)]. This effect is also evident from the fact that the highest probable velocity is higher for sample A compared to sample C, which can be attributed to lower loss of initial kinetic energy to the viscous dissipation and lower thickness [see Figs. 8(d) and 8(f)]. Even though layer C has a significantly lesser number of daughter droplets due to its low porosity, the penetrated daughter droplets have similar proportion of different ranges of droplet sizes in both the cases A and C, as shown in the experimental shadowgraphy images [see the supplementary material Fig. S2(a) and S2(d)].

Furthermore, it is interesting to note that in the case of samples layer A and $2 \times$ A, a very small number of larger size droplets ($>150 \mu\text{m}$) are also present along with the dominant $0\text{--}100 \mu\text{m}$ range daughter droplets [as shown in supplementary material Figs. S2(a) and S2(b)]. This shows a mild possibility of the presence of larger droplets even in the case of double layers when the layers have high porosity similar to layer A ($\phi \sim 17\%$). However, this effect was not significant in the case of layer C, for either single or double layer of the sample, due to its smaller pore size as well as larger fabric thickness, as shown in Fig. 8(f) and supplementary material Figs. S2(d) and S2(f). When the performance of the two samples, $3 \times$ layer A and $2 \times$ layer C, is compared, the higher fabric thickness in $3 \times$ A contributes to the lower penetration volume due to the dominant viscous dissipation. However, the penetrated daughter droplets in the case of sample $3 \times$ A have significant number of relatively larger droplets ($100\text{--}200 \mu\text{m}$) even though it is a three-layered configuration, compared to the two-layered configuration of $2 \times$ C, which is having lower porosity [see Figs. 8(g) and 8(I)]. Comparing the two samples A + C and $2 \times$ C, it is evident that even though the penetration volume percentage is similar ($\sim 0.35\%$) in both the cases, the sample A + C exhibited the presence of relatively larger-sized penetrated droplets ($>100 \mu\text{m}$) compared to the sample $2 \times$ C [Figs. 8(h) and 8(i) and supplementary material Figs. S2(e) and S2(f)]. This is attributed to the larger pore size of the layer A. The spray impingement phenomena in the case of sample $2 \times$ A, A + C, and $2 \times$ C are shown in Fig. 8. The still images of penetrated droplets in the case of different mask samples are shown in the supplementary material (see Fig. S2).

Another observation from the shadowgraphy images is that the lesser porous samples exhibit a significant amount of bounced-back volume, which is retained on top of the mask without penetration. From these experiments, it can be inferred that the lower effective porosity of the mask due to the additional number of layers leading to higher fabric thickness can lead to significantly lower volume penetration compared to the samples having similar or relatively low pore size. This is because of the dominance of the viscous dissipation effects, which resist the penetration of the droplets in the case of masks having higher t_m/ϵ ratio.

The ϕ/C ratio is effective in incorporating the effect of global parameter porosity (ϕ) on spray impingement in addition to the pore-level criteria based on the local parameters like pore size (ϵ) and fabric thickness (t_m). Additionally, the ϕ/C ratio is a good tool to estimate the extent of penetration of a spray through a given mask fabric. It is to be noted that if the pore sizes are varying drastically between the samples, the effect of ϕ on penetration will not be straightforward, as the pore size (ϵ) can affect both viscous dissipation and capillary effects. Lower pore size is needed for higher viscous dissipation and larger capillary forces that resist volume penetration. This leads to lower penetrated volume, but a significant number of smaller daughter droplets in the aerosolization range will be formed. However, low porosity and relatively higher pore size are also another option to consider for a mask as shown by Krishan *et al.*, where lower net volume penetration can be achieved with lesser extent of aerosolization effect.²⁹ In addition to all these intercoupled effects, usage of higher thickness material for mask layer is beneficial in reducing penetration volume. However, a minimum of three layers are necessary in order to reduce the effect of aerosolization, which can minimize the potentially harmful outbreak of contagious diseases.

The current experiments try to replicate the droplet sizes and velocities involved in a coughing event using a spray, to study the effects of mask properties on the droplet penetration. It is evident from the data that the droplets of different sizes ($d > \epsilon$) atomize into even smaller daughter droplets, resulting in significant aerosolization. This suggests that the penetration criteria are also valid for smaller droplet range ($d < 100 \mu\text{m}$), which contribute significantly to the aerosolized penetrated droplets [see Figs. 8(j) and 8(k)]. It is to be noted that the scope of the current experiments is only limited to the droplet dynamics of the spray impingement and its penetration through the mask. However, the effect of air flow and turbulence involved during an actual coughing event will result in the transportation of these aerosolized ejected droplets.^{37,43} This presence of air flow and turbulence increases the range of infection compared to the distances associated with the velocity of these individual penetrated droplets. Hence, the respiratory jet and turbulence effects have to be superimposed over the velocity scales of the penetrated droplets ejected, while considering the range of infection around an infected person wearing a mask.

E. Effect of mask usage by a susceptible person in the proximity

From the experiments, the penetrated droplets through the mask fabric are shown to be in lower diameter regime with a significant number of droplets in the aerosolization range. The velocity scale of the penetrated daughter droplets is in the range of 0–2 m/s. This section discusses the fate of daughter droplets ejected through a mask,

when a second manikin is placed in the path of their trajectory. Akhtar *et al.* have reported data regarding the mask efficacy in face-to-face interactions.⁵⁶ The high level of transmission and ingestion of virus through respiratory droplets from an infected person in proximity is shown by Agarwal and Bhardwaj.⁵⁷ Hence, experiments have been conducted to replicate the situation similar to social conversations and to determine the effectiveness of the mask usage. The main purpose of the experiments is to check the efficacy of mask worn by a susceptible person against aerosolized low-velocity droplets ejected from the cough of an infected person wearing mask.

The two manikins are placed at a distance of 10 cm from each other [see Figs. 9(a) and 9(b)]. The primary manikin (representing the infected person wearing mask) has been used for inducing model-cough, generated using a spray of DI water. A dark-colored dye added to the DI water for the detection of penetrated droplets. On the receiving end, the mouth portion of the secondary manikin (representing a susceptible person) has been covered by a white cloth for detection of any penetrated droplets impinging on it, and a mask is worn on top of it, as shown in Fig. 9(b). Experiments were conducted as explained in Sec. II, using the susceptible person manikin both with and without the mask, during the cough event from infected person manikin. To study the penetration specifically, all these experiments were performed using high porosity single-layer mask (layer A, $\phi \sim 17\%$).

When the mask is worn on the susceptible person, repeated cough events of the primary manikin (infected person) led to penetration [see Figs. 9(c) and 9(d)]. This is evident from the small number of

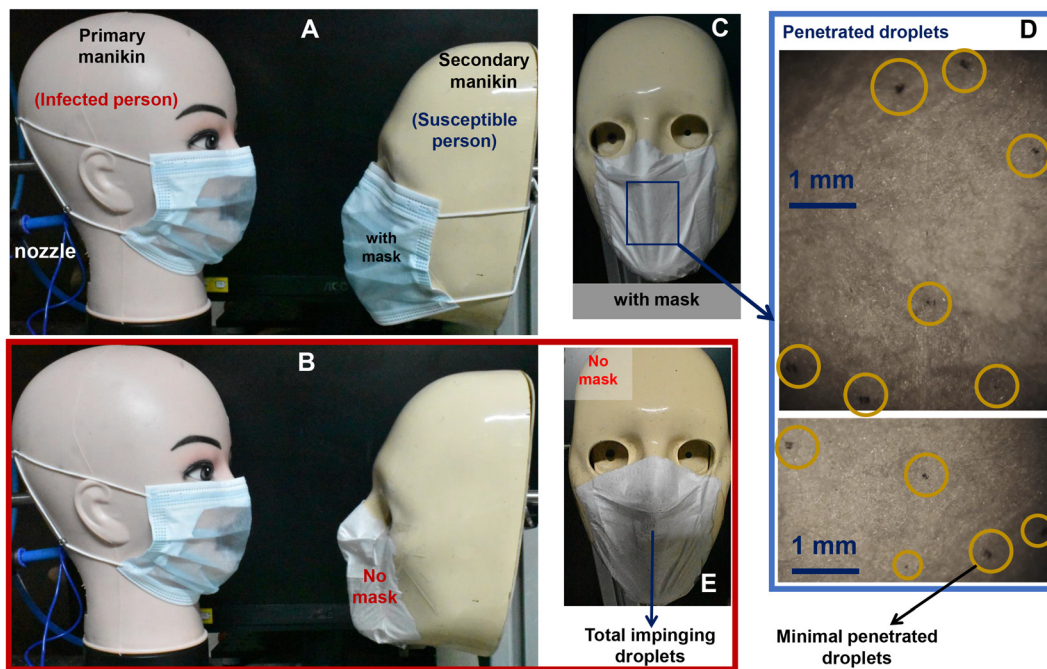


FIG. 9. Double manikin experiments to investigate the fate of penetrated droplets from primary manikin (representing infected person with mask) in the presence of secondary manikin (representing susceptible person) in the vicinity. (a) Two manikins placed at 10 cm distance with both wearing a mask, (b) two manikins facing each other with secondary manikin not wearing mask, (c) snapshot of penetrated droplets on secondary manikin wearing a mask against repeated cough cycles, (d) the zoomed-in microscopic images of the penetrated droplets on the susceptible person manikin wearing mask, showing minimal penetration, (e) snapshot of secondary manikin without wearing mask, showing total amount of impinging droplets ejected from the infected person manikin. All scale bars are shown.

penetrated droplets detected on the white cloth pasted on the mouth of the susceptible person [see Fig. 9(d)], when compared to the total number of droplets detected without the mask, as shown in Fig. 9(e). The minimal penetration through the mask of the receiving manikin is because of the reduced velocity scales (0–2 m/s) of the ejected droplets, as they pass through the mask of infected person.³⁰ However, these smaller numbers of droplets potentially can cause infection when they penetrate the mask of a susceptible person. This shows that it is not sufficient to reduce the risk of infection even if the single-layer masks are worn by both infected and susceptible persons. Thus, the experiments clearly suggest the necessity of the need of multiple layers

as well as social distancing for susceptible people, in mitigating the spread of contagious respiratory diseases.

F. Penetration dynamics of virus-emulating nanoparticle-laden surrogate respiratory droplets

From the experiments, it has been shown that the mask blocks the significant volume of cough droplets ejected out. Nevertheless, the effectiveness of mask to block the virions present in infected respiratory droplets also needs to be investigated. The temporal and

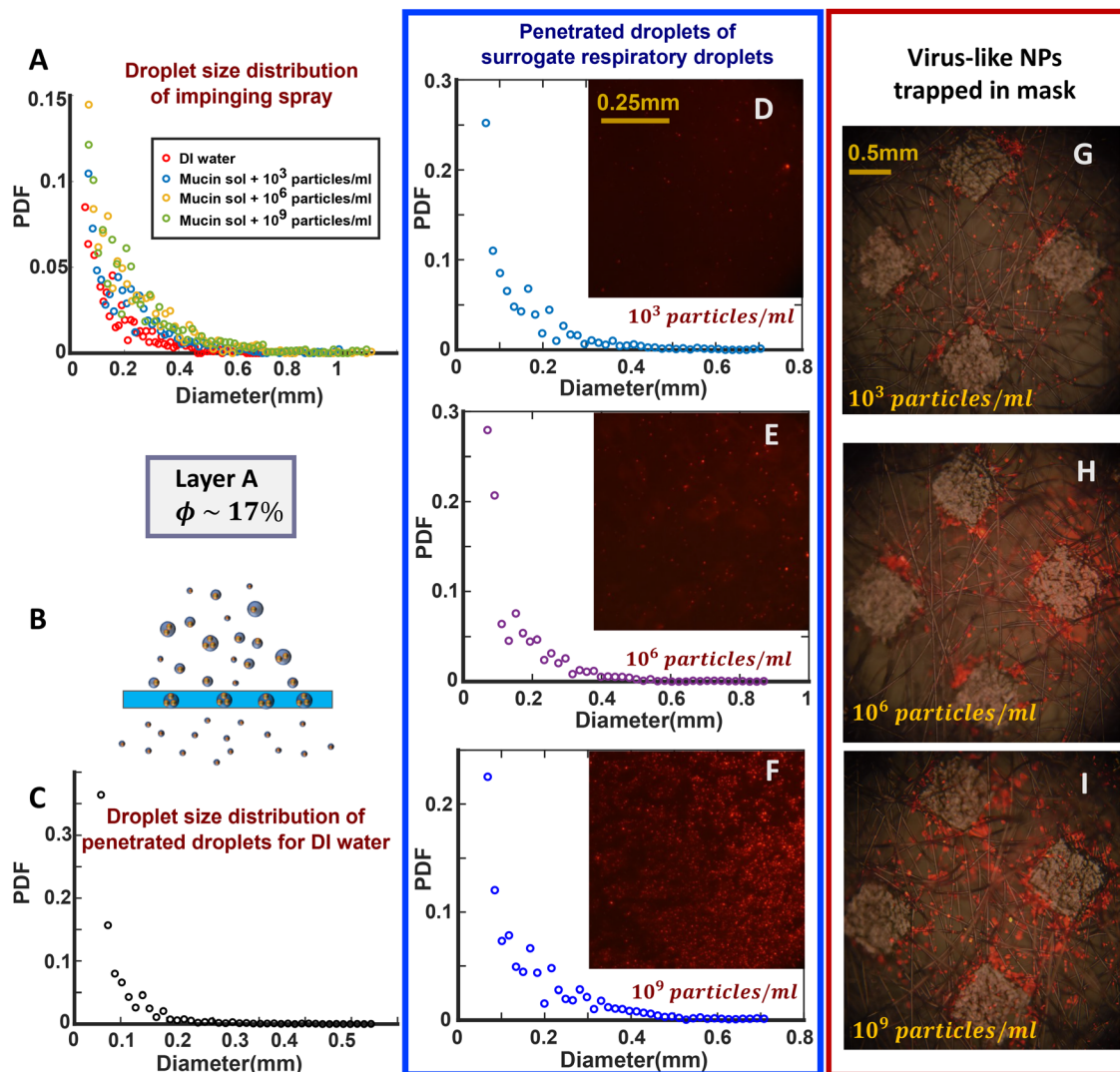


FIG. 10. (a) The impinging spray characteristics to be similar for the nanoparticle (NP)-laden mucin solution for different particle loading rates and DI water. (b) The schematic of the virus-like nanoparticle-laden spray droplet penetration has been shown. (c) The droplet size distribution of penetrated droplets through layer A for DI water. (d)–(f) The droplet size distribution (PDF) of penetrated droplets through layer A using: (d) 10^3 NP particles per ml of mucin solution, (e) 10^6 NP particles per ml of mucin solution, (f) 10^9 NP particles per ml of mucin solution. (d)–(f) The fluorescence microscopy images of virus-like nanoparticles corresponding to the penetrated droplets have also been shown as sub-figures for the respective solutions. (g)–(i) The virus-like nanoparticles (NP) trapped in the mask for particle loadings: (g) 10^3 NP particles per ml of mucin solution, (h) 10^6 NP particles per ml of mucin solution, (i) 10^9 NP particles per ml of mucin solution. (g)–(i) The overlaid bright-field and fluorescence microscopy images indicating the presence of fluorescent virus-like nanoparticles embedded in the mask. All scale bars are shown.

geometric distance of potential infection around an infected person and survivability of virus in air, based on droplet size ejected, has been discussed in the literature.^{58,59} Zhou and Zou have investigated the ingestion and deposition mechanisms of particles in the human respiratory tract and showed a dependency of deposition based on particle size.⁶⁰ The nano-sized particles showed even deposition, and the total particle deposition in the respiratory tract is shown to increase for (<0.3 – $0.4 \mu\text{m}$) particle size. This indicates the increase in the chance of infection in the case of virus particles in this range. The size of SARS-CoV-2 is shown to be ranging from 0.07 to $0.09 \mu\text{m}$.⁶¹ Hence, in order to mimic the virus particles, 100 nm polystyrene nanoparticles (R-100) at different particle loading rates, in the mucin solution (0.9% by wt. % NaCl, 0.3% by wt. % gastric mucin, 0.05% by wt. % DPPC added to DI water), have been used to replicate the virion-laden surrogate respiratory droplets, to investigate the mask filtration. These solutions mimic the fluid dynamics of virion-laden droplets, although they do not have the mechanical or chemical properties of virions.⁶ The virus-emulating nanoparticle-laden droplets are then impinged onto the face mask, and the deposition on the mask surface, as well as penetrated nanoparticles, has been identified from the fluorescence microscopy images. The fluorescence microscopy images have been superimposed on the bright-field microscopy images to show the corresponding location of the nanoparticle entrapment, on the mask layer.

The impinging spray generated from the spray orifice, using the nanoparticle-laden mucin solution at different particle loadings, has been found to exhibit similar droplet size distribution as that of DI water [see Fig. 10(a)]. Figure 10(b) shows the schematic depiction of the virus-emulating nanoparticle-laden droplet spray penetration, which shows the entrapment as well as penetration of virions through the mask. The fluorescence microscopy images of nanoparticles present in the penetrated droplets have been depicted in Figs. 10(d)–10(f). The size distribution of the penetrated droplets is observed to remain similar for the viral-loaded surrogate respiratory droplets as well [see Figs. 10(c) and 10(d)–10(f)]. Figures 10(g)–10(i) show the overlaid bright-field and fluorescence microscopy images on the impinged side of the mask, indicating the presence of trapped nanoparticles. This nanoparticle deposition on the mask indicates the entrapment of virions. This mandates the necessity to follow proper disposal methods for handling face masks after utilization. Experiments show that the entrapment, as well as penetration of virus-emulating nanoparticles, increases with increase in initial loading rates [see Figs. 10(d)–10(f) and 10(g)–10(i)]. It is further observed that there is a marginal increase in the tendency for the formation of larger-sized droplets ($\sim 400 \mu\text{m}$) at very high particle loading (10^9 particles/ml). It is evident from Figs. 10(g)–10(i) that the masks block and entrap a significant amount of nanoparticles (virions) along with the droplet volume, during the penetration. The virus-emulated nanoparticles were observed to be entrapped in the crevices and at the junction of the fibers on the mask layer. This suggests that the lower porosity of the mask contributes to the higher availability of the morphological surfaces on the mask, which are capable to entrap the virions. Thus, the lower porosity not only results in net reduction in the percentage volume penetrated through the mask, but also provides more surface area for the entrapment of nanoparticles. This further suggests that the morphology of the mask comprising different types of crevices can contribute to the virion entrapment.

IV. CONCLUSION

The droplet penetration phenomenon through a mask is dependent on both surface tension and viscous dissipation. Both the criteria are to be considered together to determine the possibility of penetration. However, the relative importance of one criterion over the other is dependent on the type of the mask and its properties like pore size and fabric thickness. In the current experiments, it is found that the viscous dissipation criterion is more suitable for samples with small pore sizes. However, these two criteria focus on the pore-level dynamics only and do not account for the penetration of the spray. Hence, a new parameter has been formulated based on the area available for the spray and spray density to estimate the possibility of penetration. This parameter (ϕ/C ratio) offers a new penetration criterion in addition to the two-step criteria, to incorporate the global effects of properties like porosity (ϕ) and spray density. This parameter can also give a qualitative estimate of the probability of penetration and extent of penetrated volume in the case of a spray. Both the two-step criteria and the ϕ/C ratio criteria are necessary to predict the penetration of a spray accurately. This parameter can give a general trend of the percentage volume penetrated; however, effect of the local parameters should also be considered for accurate estimation.

To get insight into the aerosolization during penetration, the effect of mask properties on the penetrated droplet size as well as the velocity distribution has been investigated. The lower pore size results in higher probability of the formation of droplets in the aerosolization range and lower velocity scales. The higher fabric thickness increases viscous dissipation, resulting in a higher probability for the ejected droplets to have lower velocity. This is also reflected in the case of additional layer usage due to the reduction of effective pore size as well as the increased effective fabric thickness. The effect of pore size and the combination of different mask layers has been investigated in the study. The multilayer mask will result in a significant reduction in the volume of the penetrated daughter droplets, which will reduce the amount of pathogen loading released into the surroundings. However, reduction of aerosolized droplets along with maintaining low penetration volume percentage is an ideal scenario, as small droplets can be suspended for longer durations increasing the infection potential. The current investigation gave insight into this by having a multilayer mask having combination of different layers with relatively high pore size as well as low pore size. It is to be noted that this will only be effective if the combination can result in a low penetration volume percentage. However, further investigation is necessary to get better insight into the effect of pore size.

The penetration characteristics of the spray show that all ranges of droplet diameters ($d > \epsilon$) contribute to aerosolization. The smaller droplets ($d < 100 \mu\text{m}$) tend to atomize into further smaller-sized droplets resulting in higher degree of atomization along with larger droplets ($d > 250 \mu\text{m}$). This aerosolization effect that is purely based on droplet dynamics coupled with the turbulent flow associated with respiratory jets during the cough will potentially increase the infection potential to larger distances by the transportation of aerosolized droplets. Hence, all the penetration criteria along with the turbulence effects are to be considered in estimating the potential infection zone around an infected person. It has been observed from the manikin studies that penetration is observed at the receiving end, even when both the infected and susceptible persons wear single-layer mask. This suggests that both social distancing and a multi-layered mask are necessary to efficiently block the viral-loaded respiratory droplets from spreading

the infection. Additionally, experiments show that the masks block the impinging droplets along with the virus-emulating nanoparticles. Furthermore, the data suggest that the virus-emulating nanoparticles are entrapped in the morphological crevices present on the mask.

SUPPLEMENTARY MATERIAL

See the [supplementary material](#) for the size and volume distribution of droplets expelled during cough event as given in Duguid (1946), and experimental snapshots of spray impingement phenomenon for different samples were included.

ACKNOWLEDGMENTS

The authors thank Abdur Rasheed for his help in preparation of the mucin solutions. The authors received no funding for this work.

AUTHOR DECLARATIONS

Conflict of Interest

The authors have no conflicts to disclose.

Author Contributions

S.B. and D.C. conceptualized the idea. G.V. and T.S.K. formulated experimental framework, conducted the experiments for data visualization and acquisition, and processed and analyzed the data. G.V. and S.B. developed the breakup theory. G.V., T.S.K., S.B., and A.S. developed the penetration criterion. All the relevant biological aspects were overseen and guided by D.C. S.B., and D.C., and A.S. supervised the project. Initial draft is written by G.V. G.V., and T.S.K., and S.B. contributed to final draft. All authors edited and approved the manuscript.

DATA AVAILABILITY

The data that support the findings of this study are available within the article and its [supplementary material](#).

REFERENCES

- Y. Liu, Z. Ning, Y. Chen, M. Guo, Y. Liu, N. K. Gali, L. Sun, Y. Duan, J. Cai, D. Westerdahl, X. Liu, K. Xu, K. F. Ho, H. Kan, Q. Fu, and K. Lan, "Aerodynamic analysis of SARS-CoV-2 in two Wuhan hospitals," *Nature* **582**, 557–560 (2020).
- World Health Organization, *Transmission of SARS-CoV-2: Implications for Infection Prevention Precautions Scientific Brief* (World Health Organization, 2020), pp. 1–10.
- M. Richard, J. M. A. van den Brand, T. M. Bestebroer, P. Lexmond, D. de Meulder, R. A. M. Fouchier, A. C. Lowen, and S. Herfst, "Influenza A viruses are transmitted via the air from the nasal respiratory epithelium of ferrets," *Nat. Commun.* **11**, 766 (2020).
- C. Y. H. Chao, M. P. Wan, L. Morawska, G. R. Johnson, Z. D. Ristovski, M. Hargreaves, K. Mengersen, S. Corbett, Y. Li, X. Xie, and D. Katoshevski, "Characterization of expiration air jets and droplet size distributions immediately at the mouth opening," *J. Aerosol Sci.* **40**, 122–133 (2009).
- S. Basu, P. Kabi, S. Chaudhuri, and A. Saha, "Insights on drying and precipitation dynamics of respiratory droplets from the perspective of COVID-19," *Phys. Fluids* **32**, 123317 (2020).
- A. Rasheed *et al.*, "Precipitation dynamics of surrogate respiratory sessile droplets leading to possible fomites," *J. Colloid Interface Sci.* **600**, 1–13 (2021).
- W. F. Wells, "On air-borne infection: Study II. Droplets and droplet nuclei," *Am. J. Epidemiol.* **20**, 611–618 (1934).
- R. Tellier, "Review of aerosol transmission of influenza A virus," *Emerg. Infect. Dis.* **12**, 1657–1662 (2006).
- J. P. Duguid, "The size and the duration of air-carriage of respiratory droplets and droplet-nuclei," *Epidemiol. Infect.* **44**, 471–479 (1946).
- S. Chaudhuri, S. Basu, and A. Saha, "Analyzing the dominant SARS-CoV-2 transmission routes toward an *ab initio* disease spread model," *Phys. Fluids* **32**, 123306 (2020).
- S. Chaudhuri, S. Basu, P. Kabi, V. R. Unni, and A. Saha, "Modeling the role of respiratory droplets in COVID-19 type pandemics," *Phys. Fluids* **32**, 63309 (2020).
- T. Brooks and J. C. Butler, "Effectiveness of mask wearing to control community spread of SARS-CoV-2," *JAMA* **325**, 998–999 (2021).
- C. R. MacIntyre, S. Cauchemez, D. E. Dwyer, H. Seale, P. Cheung, G. Browne, M. Fasher, J. Wood, Z. Gao, R. Booy, and N. Ferguson, "Face mask use and control of respiratory virus transmission in households," *Emerg. Infect. Dis.* **15**, 233–241 (2009).
- D. S. Hui, B. K. Chow, L. Chu, S. S. Ng, N. Lee, T. Gin, and M. T. V. Chan, "Exhaled air dispersion during coughing with and without wearing a surgical or N95 mask," *PLoS One* **7**, e50845 (2012).
- A. Konda, A. Prakash, G. A. Moss, M. Schmoldt, G. D. Grant, and S. Guha, "Aerosol filtration efficiency of common fabrics used in respiratory cloth masks," *ACS Nano* **14**, 6339–6347 (2020).
- P. Brunet, F. Lapiere, F. Zoueshtiagh, V. Thomy, and A. Merlen, "To grate a liquid into tiny droplets by its impact on a hydrophobic microgrid," *Appl. Phys. Lett.* **95**, 254102 (2009).
- W. Lewei, W. Xiao, Y. Weijie, H. Pengfei, H. Feng, and X. Zhang, "Numerical study of droplet fragmentation during impact on mesh screens," *Microfluid. Nanofluid.* **23**(12), 136 (2019).
- D. Soto, H. L. Girard, A. L. Hellico, T. Binder, D. Quéré, and K. K. Varanasi, "Droplet fragmentation using a mesh," *Phys. Rev. Fluids* **3**, 083602 (2018).
- L. Sun, S. Lin, B. Pang, Y. Wang, E. Li, X. Zu, K. Zhang, X. Xiang, and L. Chen, "Water sprays formed by impinging millimeter-sized droplets on superhydrophobic meshes," *Phys. Fluids* **33**, 092111 (2021).
- F. Yeganehdoust, R. Attarzadeh, A. Dolatabadi, and I. Karimfazli, "A comparison of bioinspired slippery and superhydrophobic surfaces: Micro-droplet impact," *Phys. Fluids* **33**, 022105 (2021).
- G. Wang, J. Gao, and K. H. Luo, "Droplet impacting a superhydrophobic mesh array: Effect of liquid properties," *Phys. Rev. Fluids* **5**, 123605 (2020).
- S. Ryu, P. Sen, Y. Nam, and C. Lee, "Water penetration through a superhydrophobic mesh during a drop impact," *Phys. Rev. Lett.* **118**, 014501 (2017).
- S. A. Kooij, A. M. Moqaddam, T. C. De Goede, D. Derome, J. Carmeliet, N. Shahidzadeh, and D. Bonn, "Sprays from droplets impacting a mesh," *J. Fluid Mech.* **871**, 489–509 (2019).
- U. Sen, T. Roy, S. Chatterjee, R. Ganguly, and C. M. Megaridis, "Post-impact behavior of a droplet impacting on a permeable metal mesh with a sharp wettability step," *Langmuir* **35**, 12711–12721 (2019).
- C. Bae, S. Oh, J. Han, Y. Nam, and C. Lee, "Water penetration dynamics through a Janus mesh during drop impact," *Soft Matter* **16**, 6072–6081 (2020).
- A. Kumar, A. Tripathy, Y. Nam, C. Lee, and P. Sen, "Effect of geometrical parameters on rebound of impacting droplets on leaky superhydrophobic meshes," *Soft Matter* **14**, 1571–1580 (2018).
- R. P. Sahu, S. Sinha-Ray, A. L. Yarin, and B. Pourdeyehimi, "Drop impacts on electrospun nanofiber membranes," *Soft Matter* **8**, 3957–3970 (2012).
- J. Xu, J. Xie, X. He, Y. Cheng, and Q. Liu, "Water drop impacts on a single-layer of mesh screen membrane: Effect of water hammer pressure and advancing contact angles," *J. Exp. Therm. Fluid Sci.* **82**, 83–93 (2017).
- B. Krishan, D. Gupta, G. Vadlamudi, S. Sharma, D. Chakravorty, and S. Basu, "Efficacy of homemade face masks against human coughs: Insights on penetration, atomization, and aerosolization of cough droplets," *Phys. Fluids* **33**, 093309 (2021).
- S. Sharma, R. Pinto, A. Saha, S. Chaudhuri, and S. Basu, "On secondary atomization and blockage of surrogate cough droplets in single- and multi-layer face masks," *Sci. Adv.* **7**, eabf0452 (2021).
- S. Bagchi, S. Basu, S. Chaudhuri, and A. Saha, "Penetration and secondary atomization of droplets impacted on wet facemasks," *Phys. Rev. Fluids* **6**, 110510 (2021).
- V. Arumuru, J. Pasa, and S. S. Samantary, "Experimental visualization of sneezing and efficacy of face masks and shields," *Phys. Fluids* **32**, 115129 (2020).

- ³³S. Verma, M. Dhanak, and J. Frankenfield, “Visualizing the effectiveness of face masks in obstructing respiratory jets,” *Phys. Fluids* **32**, 061708 (2020).
- ³⁴A. Rodriguez-Palacios, F. Cominelli, A. R. Basson, T. T. Pizarro, and S. Ilic, “Textile masks and surface covers—A spray simulation method and a universal droplet reduction model against respiratory pandemics,” *Front. Med.* **7**, 260 (2020).
- ³⁵N. H. L. Leung, D. K. W. Chu, E. Y. C. Shiu, K. H. Chan, J. J. McDevitt, B. J. P. Hau, H. L. Yen, Y. Li, D. K. M. Ip, J. S. M. Peiris, W. H. Seto, G. M. Leung, D. K. Milton, and B. J. Cowling, “Respiratory virus shedding in exhaled breath and efficacy of face masks,” *Nat. Med.* **26**, 676–680 (2020).
- ³⁶J. W. Tang, T. J. Liebner, B. A. Craven, and G. S. Settles, “A schlieren optical study of the human cough with and without wearing masks for aerosol infection control,” *J. R. Soc. Interface* **6**, S727–S736 (2009).
- ³⁷C. J. Kähler and R. Hain, “Fundamental protective mechanisms of face masks against droplet infections,” *J. Aerosol Sci.* **148**, 105617 (2020).
- ³⁸J. Pan, C. Harb, W. Leng, and L. C. Marr, “Inward and outward effectiveness of cloth masks, a surgical mask, and a face shield,” *Aerosol Sci. Technol.* **55**(6), 718–733 (2021).
- ³⁹D. A. Rothamer, S. Sanders, D. Reindl, and T. H. Bertam, “Strategies to minimize SARS-CoV-2 transmission in classroom settings: Combined impacts of ventilation and mask effective filtration efficiency,” *Sci. Technol. Built Environ.* **27**, 1181–1203 (2021).
- ⁴⁰S. R. Lustig, J. J. H. Biswakarma, D. Rana, S. H. Tilford, W. Hu, M. Su, and M. S. Rosenblatt, “Effectiveness of common fabrics to block aqueous aerosols of virus-like nanoparticles,” *ACS Nano* **14**(6), 7651–7658 (2020).
- ⁴¹T. Dbouk and D. Drikakis, “On respiratory droplets and face masks,” *Phys. Fluids* **32**, 063303 (2020).
- ⁴²D. Maggiolo and S. Sasic, “Respiratory droplets interception in fibrous porous media,” *Phys. Fluids* **33**, 083305 (2021).
- ⁴³T. Dbouk and D. Drikakis, “On coughing and airborne droplet transmission to humans,” *Phys. Fluids* **32**, 053310 (2020).
- ⁴⁴W. G. Lindsley, W. P. King, R. E. Thewlis, J. S. Reynolds, K. Panday, G. Cao, and J. V. Szalajda, “Dispersion and exposure to a cough-generated aerosol in a simulated medical examination room,” *J. Occup. Environ. Hyg.* **9**(12), 681–690 (2012).
- ⁴⁵X. Xie, Y. Li, H. Sun, and L. Liu, “Exhaled droplets due to talking and coughing,” *J. R. Soc. Interface* **6**, S703–S714 (2009).
- ⁴⁶X. Xie, Y. Li, A. T. Y. Chwang, P. L. Ho, and W. H. Seto, “How far droplets can move in indoor environments—Revisiting the Wells evaporation–falling curve,” *Indoor Air* **17**, 211–225 (2007).
- ⁴⁷R. Mittal, R. Ni, and J. H. Seo, “The flow physics of COVID-19,” *J. Fluid Mech.* **894**, F2 (2020).
- ⁴⁸J. Yan, M. Grantham, J. Pantelic, P. J. B. de Mesquita, B. Albert, F. Liu, S. Ehrman, D. K. Milton, and E. Consortium, “Infectious virus in exhaled breath of symptomatic seasonal influenza cases from a college community,” *Proc. Natl. Acad. Sci. U. S. A.* **115**(5), 1081–1086 (2018).
- ⁴⁹C. D. Zangmeister, J. G. Radney, E. P. Vicenzi, and J. L. Weaver, “Filtration efficiencies of nanoscale aerosol by cloth mask materials used to slow the spread of SARS-CoV-2,” *ACS Nano* **14**(7), 9188–9200 (2020).
- ⁵⁰T. Zhang, *Study on Surface Tension and Evaporation Rate of Human Saliva, and Water Droplets* (West Virginia University, 2011).
- ⁵¹K. Vontas, C. Boscaroli, M. Andreadaki, A. N. Georgoulas, C. Crua, J. H. Walther, and M. Marengo, “Droplet impact on suspended metallic meshes: Effects of wettability, Reynolds and Weber numbers,” *Fluids* **5**, 81 (2020).
- ⁵²E. P. Vejerano and L. C. Marr, “Physico-chemical characteristics of evaporating respiratory fluid droplets,” *J. R. Soc. Interface* **15**, 20170939 (2018).
- ⁵³T. C. De Goede, A. M. Moqaddam, K. C. M. Limpens, S. A. Kooij, D. Derome, J. Carmeliet, N. Shahidzadeh, and D. Bonn, “Droplet impact of Newtonian fluids and blood on simple fabrics: Effect of fabric pore size and underlying substrate,” *Phys. Fluids* **33**, 033308 (2021).
- ⁵⁴S. H. Smith, G. A. Somsen, C. V. Rijn, S. Kooij, L. van der Hoek, R. A. Bem, and D. Bonn, “Aerosol persistence in relation to possible transmission of SARS-CoV-2,” *Phys. Fluids* **32**(10), 107108 (2020).
- ⁵⁵P. Kulkarni, P. Baron, and K. Willeke, *Aerosol Measurement: Principles, Techniques and Applications*, 3rd ed. (John Wiley & Sons, Inc., Hoboken, NJ, 2011), pp. 107–128.
- ⁵⁶J. Akhtar, A. L. Garcia, L. Saenz, S. Kuravi, F. Shu, and K. Kota, “Can face masks offer protection from airborne sneeze and cough droplets in close-up, face-to-face human interactions? A quantitative study,” *Phys. Fluids* **32**, 127112 (2020).
- ⁵⁷A. Agrawal and R. Bhardwaj, “Probability of COVID-19 infection by cough of a normal person and a super-spreader,” *Phys. Fluids* **33**, 031704 (2021).
- ⁵⁸S. K. Das, J. E. Alam, S. Plumari, and V. Greco, “Transmission of airborne virus through sneezed and coughed droplets,” *Phys. Fluids* **32**, 097102 (2020).
- ⁵⁹S. W. X. Ong, Y. K. Tan, P. Y. Chia, T. H. Lee, O. T. Ng, M. S. Y. Wong, and K. Marimuthu, “Air, surface environmental, and personal protective equipment contamination by severe acute respiratory syndrome coronavirus 2 (SARS-CoV-2) from a symptomatic patient,” *JAMA* **323**, 1610 (2020).
- ⁶⁰M. Zhou and J. Zou, “A dynamical overview of droplets in the transmission of respiratory infectious diseases,” *Phys. Fluids* **33**, 031301 (2021).
- ⁶¹B. U. Lee, “Minimum sizes of respiratory particles carrying SARS-CoV-2 and the possibility of aerosol generation,” *Int. J. Environ. Res. Public Health* **17**(19), 6960 (2020).